UCLA-PPG--1380

DE92 006426

PISCES Program*

Progress Report for 1990-1991 on

Plasma-Materials Interactions and Edge-Plasma Physics Research

Edited by Y.Hirooka

UCLA PPG# 1380 December, 1991

*Supported by the U.S. Department of Energy under grant #DE-FG03-86ER-52134.

This report has been contributed by the PISCES team at UCLA:

Research Staff	Support Staff	Graduate Student
R.W.Conn (PI)	T.Sketchley	R.Lehmer
Y.Hirooka (PI)	G.Gunner	Y.Tao
L.Schmitz	S.Keller	L.Blush
R.Doerner	L.Chousal	P.Chia
G.Chevalier	P.Luong	S.Jou
M.Khandagle	M.C.Srinivasan	
Y.Ra	H.Sasanpour,	

and collaborations have been done with:

the ALT-II team at UCLA : G.Tynan;
the PMI-theory group at UCLA: F.Najmabadi, A.Grossman, M.Day, B.Merriman;
the Fusion Power Program at ANL: J.Brooks;
the Tokamak de Varennes team at CCMF, Canada: C.Boucher, B.Gregory et al.;
the Wendelstein VII-AS team, IPP Garching, Germany: P.Grigull et.al.;
the tokamak laboratory at UCLA: R.J.Taylor, P.Pribyl; and
Toyo Tanso Inc. Ltd., Japan: T.Matsuda, T.Sogabe.

TABLE OF CONTENTS

1. PISCES Program

OBJECTIVES OF THE PISCES-PROGRAM

Materials and Surface Physics

To investigate and characterize the behavior of materials under plasma bombardment

↓

To develop materials for plasma-facing components in fusion reactors

Edge-Plasma Physics

To investigate and understand the behavior of plasmas interacting with surfaces

↓

To develop techniques to control the plasma flow and associated heat flux to surfaces

THE PISCES TEAM AT UCLA

Faculty Staff: Prof. R.W.Conn (Principal Investigator)
IPFR Director

Research Staff: (1) Surface and Materials Physics:

Dr. Y.Hirooka (Principal Investigator)
Principal Institute Scientist

Dr. M.Khandagle
Postdoctral fellow

(2) Plasma Spectroscopy:

Dr. G.Chevalier
Postdoctral fellow

Dr. Y.Ra
Postdoctral fellow

(3) Edge-Plasma Physics:

Dr. L.Schmitz
Institute Scientist

Dr. R.Doerner
Institute Scientist

Support Staff: (1) Computing: M.C.Srinivasan
H.Sasanpour

(2) Mechanical: T.Sketchley
S.Keller
L.Chousal

(3) Electrical: G.Gunner
P.Loung

Graduate Students: R.Lehmer, L.Blush, C.Ping, Y.Tao, S. Jou

HIGHLIGHTS IN THE PROGRAM HISTORY

1984 - PISCES-program funded by DOE-OFE.
* PISCES-A facility in operation.

1985 - First experimental demonstration of the redeposition effects in PISCES-A.
* AES-SIMS surface analysis station constructed.

1986 - First pump limiter simulation experiment in PISCES-A.
* Optical diagnostics established for plasma spectroscopy.

1987 - First off-line hydrogen plasma pumping experiments in PISCES-A.
- First off-line biased limiter (**E** x **B**) experiments in PISCES-A.
* PISCES-B design started.

1988 - CCT experiments started in collaboration with Tokamak Lab., UCLA.
- First plasma spectroscopy experiment in PISCES-A with KFA-Jülich.
* SEM-EDX installed (UCLA-TRW laboratory).

1989 - First RF Ponderomotive Force experiment in PISCES-A with IPP, Nagoya.
- First gaseous divertor experiment in PISCES-A.
- First boronized graphite experiment in PISCES-B.
* PISCES-B with in-situ AES-SIMS completed.

1990 - Systematic evaluation boronized graphites with Toyo Tanso, SNLs, NEL.
- First fully poloidal measurements of plasma edge flows in CCT.
- Experimental proof of the radial electric field effect on plasma turbulence
* PISCES-C (Jr.) constructed.

1991 - Solid Target Boronization applied in the Tokamak de Varennes
- First W-coatings erosion experiment in PISCES-B
- H-mode transition physics experiment in PISCES-A
- First observation of large scale dc convection patterns during L-mode in CCT
* PISCES-upgrade design started.

PISCES COLLABORATION IN 1990-1991

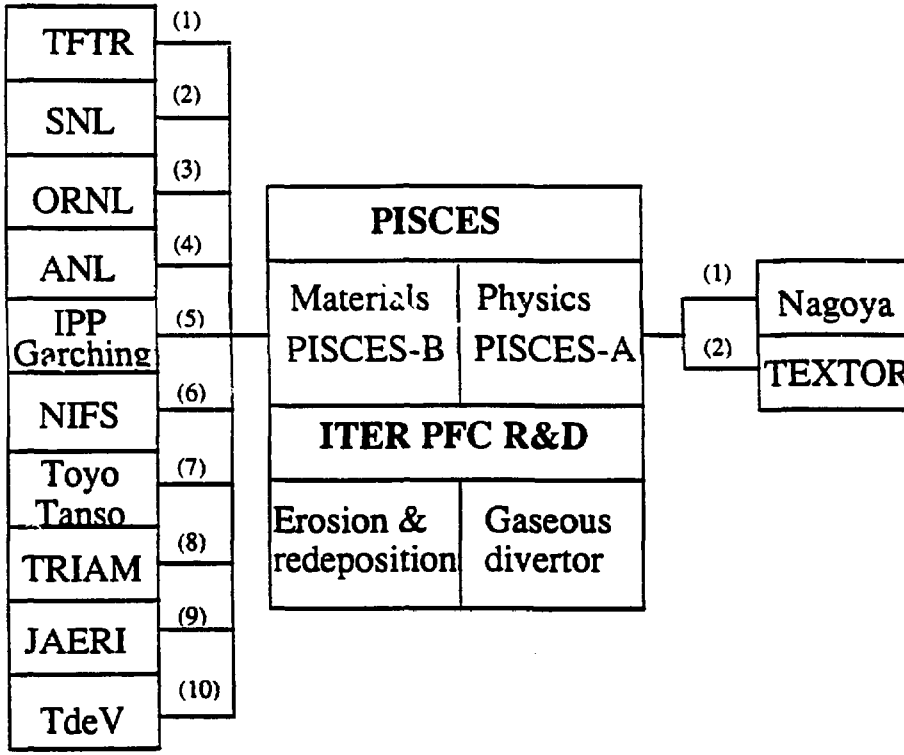

Materials collaboration:

(1) DT-Materials Physics Meeting,
(2) W-coatings: D-inventory
(3) Neutron irradiation of boronized graphites
(4) REDEP analysis on impurity transport exps.
(5) Boronized graphite limiter in W7AS
(6) RES exps. on C-C composites for LHS
(7) Boronized C-C composite development
(8) High-Z materials erosion experiment
(9) Acively-cooled divertor element tests
(10) Solid target boronization in TdeV

Plasma physics collaboration:

(1) ECH in PISCES-A
(2) RF Ponderomotive force limiter

PUBLICATIONS FROM THE PISCES-TEAM

(1) "Plasma surface interaction experimental facility (PISCES) for materials and edge physics studies"
D.M.Goebel, G.Campbell and R.W.Conn
J.Nucl.Mater. 121(1984)277.

(2) "Observation of enhanced particle removal rates in pump limiter simulation experiments"
D.M.Goebel and R.W.Conn
J.Nucl.Mater. 129&129(1984)249.

(3) "Large area lunthanum hexaboride electron emitter"
D.M.Goebel,Y.Hirooka and T.A.Sketchley
Rev.Sci.Instrum. 56(1985)1717.

(4) "Large area lanthanum molybdenum electron emitters"
D.M.Goebel, Y.Hirooka and G.A.Campbell
Rev.Sci.Instrum. 56(1985)1888.

(5) "Quasi-thermodynamic prediction of hydrogen reemission behavior from titanium films"
Y.Hirooka, D.M.Goebel and R.W.Conn
J.Nucl.Mater. 135(1985)82.

(6) "Materials erosion and redeposition studies at the PISCES facility - net erosion under redeposition"
Y.Hirooka, D.M.Goebel, R.W.Conn, W.K.Leung and G.A.Campbell
J.Nucl.Mater. 141-143(1986)193.

(7) "Erosion and redeposition experiments in the PISCES facility"
D.M.Goebel, Y.Hirooka, R.W.Conn, W.K.Leung, G.A.Campbell, J.Bohdansky, K.L.Wilson, W.Bauer, R.A.Causey, A.E.Pontau, A.R.Krauss, D.M.Gruen and M.H.Mendelsohn
J.Nucl.Mater. 145-147(1987)61.

(8) "High plasma-flux elevated temperature sputtering of Cu-Li alloys"
A.R.Krauss, D.M.Gruen, M.H.Mendelsohn, R.W.Conn, D.M.Goebel, Y.Hirooka and W.K.Leung
J.Nucl.Mater. 145-147(1987)401.

(9) "Materials surface modification by plasma bombardment under simultaneous erosion and redeposition conditions"
Y.Hirooka, D.M.Goebel, R.W.Conn, G.A.Campbell, W.K.Leung, K.L.Wilson. R.A.Causey, M.H.Morse and J.Bohdansky
Nucl. Instr. & Methods-B 23(1987)458.

(10) "Behavior of graphite under heat load and in contact with a hydrogen plasma"
J.Bohdandsky, C.D.Croessmann, J.Linke, J.M.McDonald, D.H.Morse, A.E.Pontau, R.D.Watson and J.B.Whitley , D.M.Goebel, Y.Hirooka, K.Leung, R.W.Conn, J.Roth, W.Ottenberger and H.E.Kotzlowsky
Nucl.Instr. & Methods-B 23(1987)527.

(11) "Temperature and composition dependence of the high flux plasma sputtering yield of Cu-Li binary alloys"
A.R.Krauss, M.H.Mendelsohn, D.M.Gruen, R.W.Conn, D.M.Goebel,Y.Hirooka, W.K.Leung and J.Bohdansky
Nucl.Instr. &Methods-B 23(1987)511.

(12) "Hydrogen pumping and release by graphite under high flux plasma bombardment"
Y. Hirooka, W. K. Leung, R. W. Conn, D. M. Goebel, B. LaBombard and R. E. Nygren
J. Vac. Sci. & Technol.-A 6(1988)2965.

(13) "Erosion of graphite by high flux hydrogen plasma bombardment"
D. M. Goebel, J. Bohdansky, R. W. Conn, Y. Hirooka, B. LaBombard, W. K. Leung, R. E. Nygren, J. Roth and G. R. Tynan
Nuclear Fusion 28(1988)1041.

(14)"Deuterium pumping and erosion behavior of selected graphite materials under high flux plasma bombardment in PISCES-A"
Y.Hirooka, R.W.Conn, D.M.Goebel, B.LaBombard, W.K.Leung, R.E.Nygren and Y.Ra
J.Nucl. Mater. 163-165(1988).

(15) "Erosion and Redeposition Behavior of selected NET-candidates under high-flux plasma bombardment in PISCES-A"
E.Franconi, Y.Hirooka, R.W.Conn, B.LaBombard, W.K.Leung and R.E.Nygren
J.Nucl.Mater 163-165(1989).

(16) "Presheath profiles in simulated tokamak edge plasmas"
B.LaBombard, R.W.Conn, Y.Hirooka, R.Lehmer, W.K.Leung, R.E.Nygren, Y.Ra, G.Tynan
J.Nucl.Mater. 162-164 (1989)314.

(17) "Erosion and redeposition of graphite by hydrogen plasmas"
D.M.Goebel, J. Bohdansky, R.W. Conn, Y. Hirooka, B. LaBombard,W. K. Leung, R. E. Nygren and G.R.Tynan
Fusion Technol. 15(1989)102.

(18) "An in-situ spectroscopic erosion yield measurement and its applicationas to sputtering and surface morphology alterations"
W.K.Leung, Y.Hirooka, R.W.Conn, D.M.Goebel, B.LaBombard and R.E.Nygren
J.Vac. Sci. & Technol.-A. 7(1989)21.

(19) "In-situ spectroscopic measurements of erosion behavior of TFTR-redeposited carbon materials under high-flux plasma bombardment in PISCES-A"
Y.Hirooka, A.Pospieszczyk, R.W.Conn, B.LaBombard, B.Mills, R.E.Nygren
Presented at 35th National Symposium of American Vacuum Society, Atlanta, 1988
J.Vac. Sci. & Technol.-A 7(1989)1070.

(20) "Hydrogen isotope trapping on graphite collectors during an isotope exchange experiment in the Tokamak Fusion Test Reactor"
S.J.Kilpatrick, R.E.Nygren, W.R.Wampler, M.Ulrickson, H.F.Dylla, D.M.Manos, A.T. Ramsey, and Y.Hirooka
J.Vac.Sci. & Technol.-A 7(1989)1087.

(21) "Spectroscopic studies of carbon impurities in PISCES-A"
Y.Ra, A.Pospieszczyk, Y.Hirooka, W.K.Leung, R.W.Conn
J.Vac.Sci.& Technol.-A8(1990)1783.

(22) "A new plasma-surface interactions research facility: PISCES-B and first materials erosion experiments on bulk-boronized graphite"
Y.Hirooka, R.W.Conn, T.Sketchley, W.K.Leung, R.Doerner, J.Elvurm, G.Gunner, M.Khandagel, R.Lehmer, P.Luong, Y.Ra, L.Schmitz and G.Tynan
J.Vac.Sci.&Technol.-A8 (1990)1790.

(23) "Radiation-enhanced sublimation of graphite in PISCES-experiments"
R.Nygren, J.Bohdansky, A.Pospieszczyk, R.Lehmer, Y.Ra, R.W.Conn, R.Doerner, Y.Hirooka, W.K.Leung, and L.Schmitz
J.Vac.Sci.&Technol.-A8 (1990)1778.

(24) "An electrostatic barrier scrape-off Layer for control of core plasma effluxes in tokamaks"
B. LaBombard, R.W. Conn, G. Tynan,
Plasma Physics and Controlled Fusion 32(1990)483.

(25) "An Omegatron mass-spectrometer for plasma ion species analysis"
E.Y.Wang, L.Schmitz, Y.Ra, B.Labombard, R.W.Conn
Rev.Sci.Instr. 61(1990)2155.

(26) "Bulk-boronized graphites for plasma-facing components in ITER"
Y.Hirooka, R.W.Conn, R.Causey, D.Croessmann, R.Doerner, D.Holland, M.Khandagle, T.Matsuda, G.Smolik, T.Sogabe, J.Whitely, K.Wilson
J.Nucl.Mater. 176&177(1990)473.

(27) "Development of bulk-boronized graphites for fusion reactor applications"
T.Sogabe, T.Matsuda, H.Ogura, Y.Hirooka, M.Khandagle and R.W.Conn,
Proc. Int.Symp. on Carbon, Tsukuba, Nov. 1990, page 886.

(28) "Evaluation of bulk-boronized graphite as a plasma-facing material in fusion devices"
Y.Hirooka, R.W.Conn, T.Sogabe, T.Matusda, H.Ogura
Proc. Int.Symp. on Carbon, Tsukuba, Nov. 1990, page 890.

(29) "Experimental simulation of the gaseous divertor concept in PISCES-A"
L.Schmitz, R.Lehmer, G.Chevalier, G.Tynan, P.Chia, R.Doerner, R.W.Conn
J.Nucl.Mater. 176&177(1990) 522.

(30) "Materials analysis of TEXTOR limiter tiles"
R.Doerner, B.Mills, E.Wallura, D.S.Walsh, G.Chevalier, R.W.Conn, K.H.Dipple, B.L.Doyle, H.G.Esser, K.H.Finken, D.Gray, Y.Hirooka, K.Koizlik, A.Miyahara, R.A.Moyer, J.G.Watkins, J.Winter
J.Nucl.Mater. 176&177(1990)954.

(31) "Experimental proof of a novel RF limiter concept in PISCES-A"
T.Shoji, A.Grossman, R.Conn, Y.Hirooka, R.Lehmer, W.Leung, L.Schmitz, G.Tynan
J.Nucl.Mater. 176&177(1990)830.

(32) "Performance of boron/carbon first wall materials under fusion relevant conditions"
J.Linke, H.Bolt, R.Doerner, H.Grübmeier, Y.Hirooka, H.Hoven, C.Mingam, H.Schlze, M.Seki, E.Wallura, T.Weber, J.Winter
J.Nucl.Mater. 176&177(1990)856.

(33) "Chemical erosion of selected carbon-carbon composites under high-flux hydrogen plasma bombardment in PISCES-B'
A.Sagara, Y.Hirooka, R.W.Conn, A.Miyahara, G.Chevalier, R.Doerner, M.Khandagle and N.Noda
Proc. 16th SOFT conf., London, Sep. 3-7th, 1990.

(34) "Hydrogen and deuterium plasma interactions with brazed first wall elements"
I.Smid, E.Wallura, J.Winter, H.Nickel, R.Doerner, Y.Hirooka, R.W.Conn, W.Jager, M.Grasserbauer, E.Kny, N.Rehis
Proc. 16th SOFT conf., London, Sep. 3-7th, 1990.

(35) "Applications of SiC and B4C coat-mix material: a new candidate for plasma-facing components"
C.Mingam, R.W.Conn, F.Dias, R.Doerner, Y.Hirooka, J.Linke, H.Nickel
Proc. 16th SOFT conf., London, Sep. 3-7th, 1990.

(36) "Enhanced confinement in CCT and PISCES-A in the presence of radial electric fields"
R.Taylor, R.W.Conn, B.Fried, R.Lehmer, J.Liberati, P.Pribyl, LSchmitz, G.Tynan, and B.Wells
Proc. 13th Int.Conf.on Plasma Physics and Controlled Fusion Research, Washinton-DC, 1990, IAEA-CN-53/A-6-5.

(37) "Pumped diverters and limters for tokamaks"
R.W.Conn
Fusion Eng. and Design. 14(1991)81.

(38) "Interactions of bulk-boronized graphites with deuterium plasmas in PISCES-B"
Y.Hirooka, R.W.Conn, M.Khandagle, G.Chevalier, T.Sogabe, T.Matsuda, H.Ogura, H.Toyoda, H.Sugai
Fusion Technol. 19(1991)2059.

(39) "Ohmic and H-Mode Transport in the CCT Tokamak Edge Plasma"
G.R.Tynan, R.W.Conn, R.Doerner, R.Lehmer and LSchmitz
Proc. 18th Eurpean Conf. on Controlled Fusion, Berlin 1991, D-23(III-89)

(40) "Steady-state convection and fluctuation-driven particle transport in the tokamak H-mod transition"
G.R.Tynan, L.Schmitz, R.W.Conn, R.Doerner, R.Lehmer
To be published in Phys.Rev.Lett.

(41) "Solid Target Boronization in the Tokamak de Varennes"
Y.Hirooka, C.Boucher, R.W.Conn, B.Gregory, M.Khandagle, E.Knystautas, T.Matsuda, R.W.Paynter, G.G.Ross, B.Stansfield
To be published in Nucl. Fusion.

(42) "EDX, AES and XPS analysis of boronized graphites developed for plasma-facing components for fusion devices"
M.Khandagle, Y.Hirooka, T.Sogabe, T.Matsuda, R.Arghavani, and R.W.Conn
To be published Surface Science.

(43)"Spectroscopic studies of chemical sputtering of graphite due to hydrogen and oxygen plasma bombardment"
Y.Ra, Y.Hirooka, L.Schmitz and R.W.Conn.
To be published in J.Chem.Phys.

2. PISCES Facilities

PISCES-A: A Versatile Facility for Plasma Edge Physics Studies

The PISCES-A facility[1] (Fig. 1) has been extensively used for Plasma-Materials Interaction studies and is currently devoted to boundary layer physics experiments, edge plasma turbulence and transport studies, biased limiter and divertor simulation experiments, and the testing of novel divertor and edge management concepts. The plasma source consists of a hot LaB_6 cathode with an annular, water-cooled copper anode and attached drifttube. The vacuum system includes four turbo-molecular pumps with a pumping speed of 1500 l/s each. The main diagnostics include: (1) motor-driven water-cooled Langmuir probes; (2) a fast scanning probe capable of measuring radial density, floating and plasma potential, as well as flow velocity and Mach number profiles; (3) a 1.3 m Czerny-Turner monochromator with OMA system; (4) a fast reciprocating probe for density and potential fluctuation measurements; (5) several baratron and ionization gauges for neutral pressure measurements; (6) a CID camera; (7) an IR surface temperature monitor. A CAMAC crate with slow and fast data loggers and a Micro Vax computer system is used for data acquisition and processing.

Differential pumping is employed to achieve a neutral gas pressure of $2x10^{-4}$ - 10^{-2} torr in the plasma source, while keeping the main chamber pressure between $6x10^{-5}$ and $2x10^{-3}$ torr. Plasma is produced in H_2, D_2, He, and Ar gas. Plasma densities of 10^{11} - $3x10^{12}$ cm^{-3} in hydrogen and helium, and up to $3x10^{13}$ cm^{-3} in argon have been achieved. The electron temperature is in the range of 3 - 30 eV.

Presently, the PISCES-A plasma source is converted for higher density hydrogen operation in order to study plasma plugging effects in the gaseous divertor simulation experiment (described in detail in a separate section). Pulsed operation will enable us to operate at a discharge current as high as 250 A. The differential pumping capability is increased by installing a second turbumolecular pump at the plasma source. This allows plasma production at higher neutral pressure while maintaining high electron temperature and ionization efficiency. The diagnostic systems are modified for pulsed plasma data acquisition.

The plasma diameter can be adjusted beween 3 and 10 cm by three independent magnet coils located in the source region. The main chamber magnetic field (variable between 100 and 1800 gauss) is produced by four water-cooled coils.

The PISCES-A chamber provides good diagnostic access. The fast scanning probe system has been extensively used for 2-D and 3-D mapping of plasma density and potential profiles during biased limiter and divertor simulation experiments and tests of magnetized probe theory and presheath measurements.

[1]D. M. Goebel, G. Campbell, R. W. Conn, J. Nucl. Mater. 121 (1984) 277

Fig. 1 A schematic diagram of the PISCES-A facility.

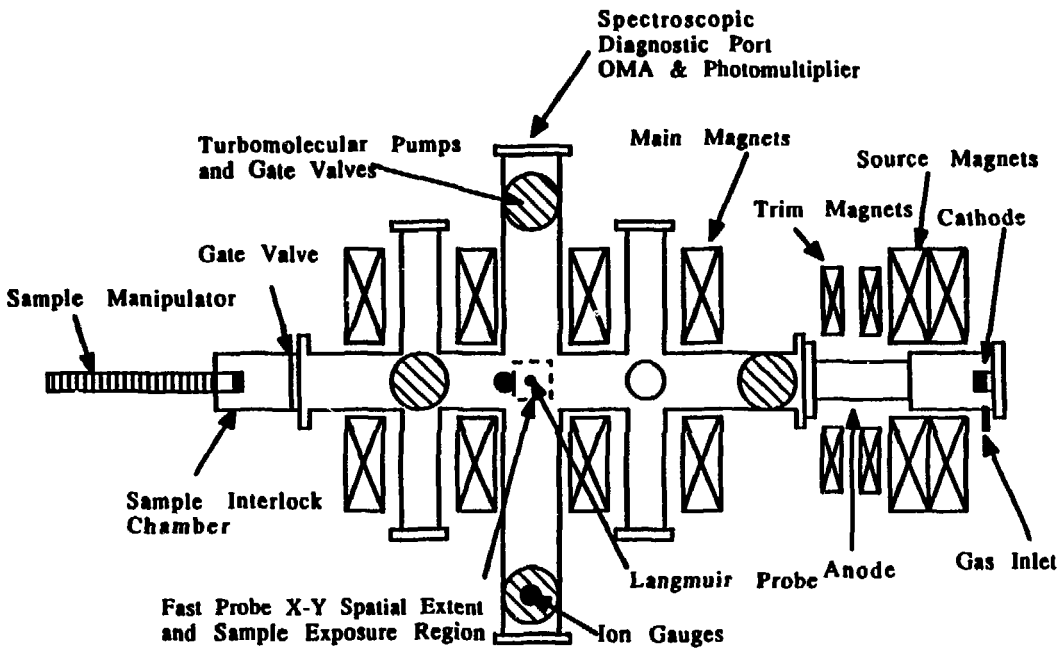

PISCES-B Mod.: Improved Plasma Operation for PSI-Experiments

The PISCES-B facility [1] has been the primary off-line (non-tokamak) plasma-surface interactions research facility operating at UCLA since 1989. The PISCES-B facility is designed for fully diagnosed PSI-experiments. A schematic diagram of the facility is shown in Fig. 1. Important features are: (1) ultra-high vacuum conditions are achievable with a total pressure of the order of 10^{-8} Torr; (2) 10 line-of-sight ports are available on the main chamber and are installed with surface diagnostics, for example, optical pyrometers focused at the sample surface; (3) a differentially pumped residual gas analyzer (RGA) to monitor gaseous plasma-surface interactions products; (4) a temperature-controlled (RT-1800°C) sample probe; (5) In-situ surface analysis station with: Auger Electron Spectroscopy (AES), X-ray induced Photoelectron Spectroscopy (XPS) and Secondary Ion Mass Spectrometry (SIMS); (6) a 1.3 m monochromator coupled with an optical multi channel analyzer (OMA) for in-situ spectroscopic analysis of impurities due to sputtering; (7) an ultra-violet (UV) spectrometer; (8) scanning Langmuir (single and double) probes.

In 1991 the heat removal efficiency in the plasma generator of PISCES-B has been improved, so that more heat load can be handled to sustain steady-state plasmas. The maximum density for the hydrogen plasma is of the order of 10^{13} cm^{-3} and that for the argon plasma is of the order of 10^{14} cm^{-3}. Both are about one order of magnitude higher than those achieved in the previous plasma generator. The electron temperature range explored so far is from 5 to 30 eV. Data taken by a fast-injection double-probe indicate relatively uniform profiles of plasma density and electron temperature over a circular area with a diameter of 5 cm. Plasma densities and electron temperatures are plotted in Fig. 2. The new regime of plasma operation in PISCES-B Mod. is more relevant to the PSI-conditions to be seen in the divertor in future fusion reactors such as ITER.

For PISCES-B Mod., the total power used to generate hydrogen plasmas with densities of around 10^{13} cm^{-3} is about 40 kW. The average heat removal rate through the water-cooled copper anode in the plasma generator is estimated to be 20 W/cm^2, which is only a fraction of the maximum heat removal capability one can achieve for water-cooled copper components. Therefore, the plasma performance can be improved even further if a larger power source is available. Upgrading of the power supply is under way.

---

[1] Y.Hirooka et al. J.Vac.Sci. & Technol. A8, 1790 (1990).

Fig. 1 A schematic diagram of the PISCES-B facility.

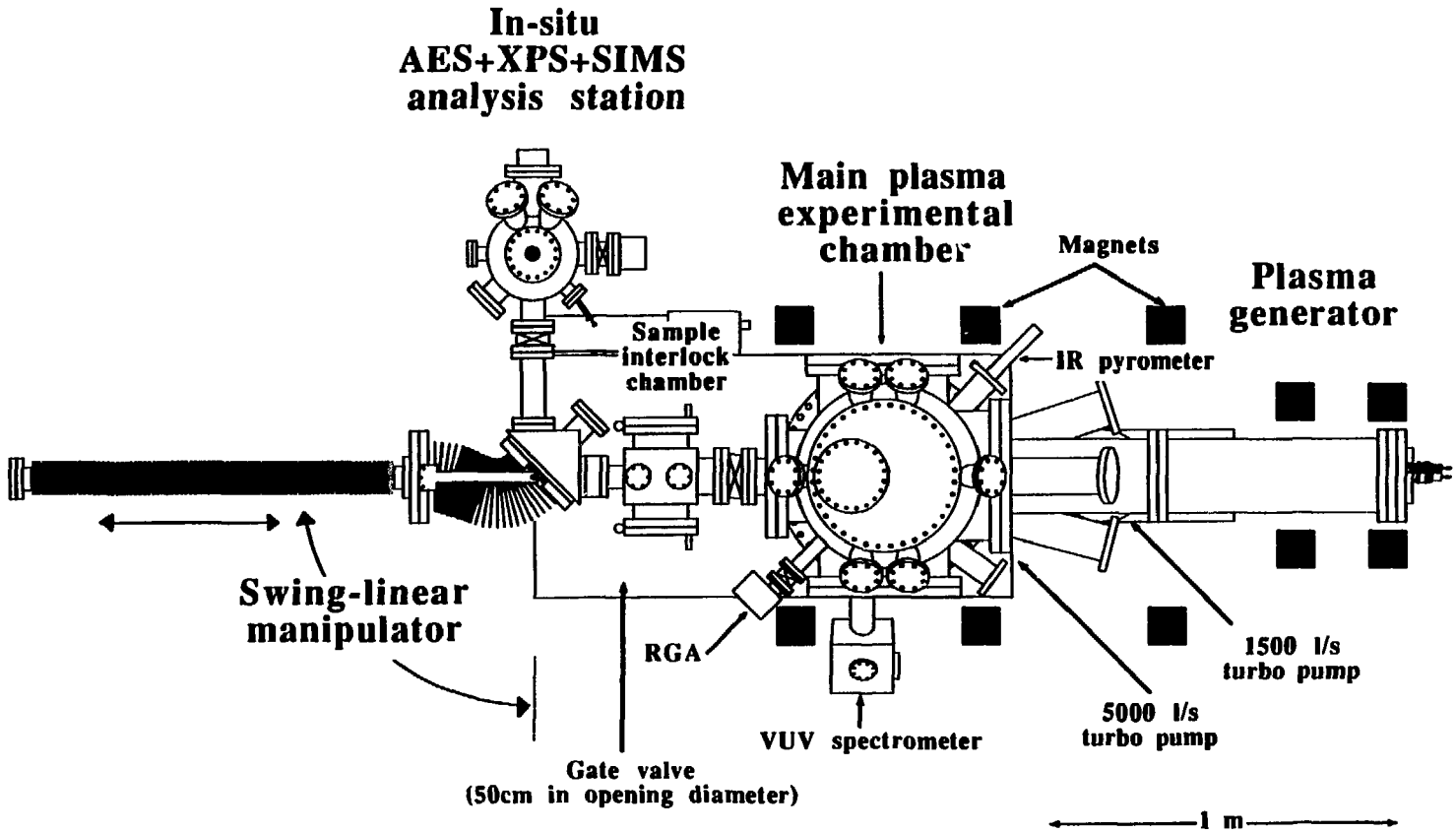

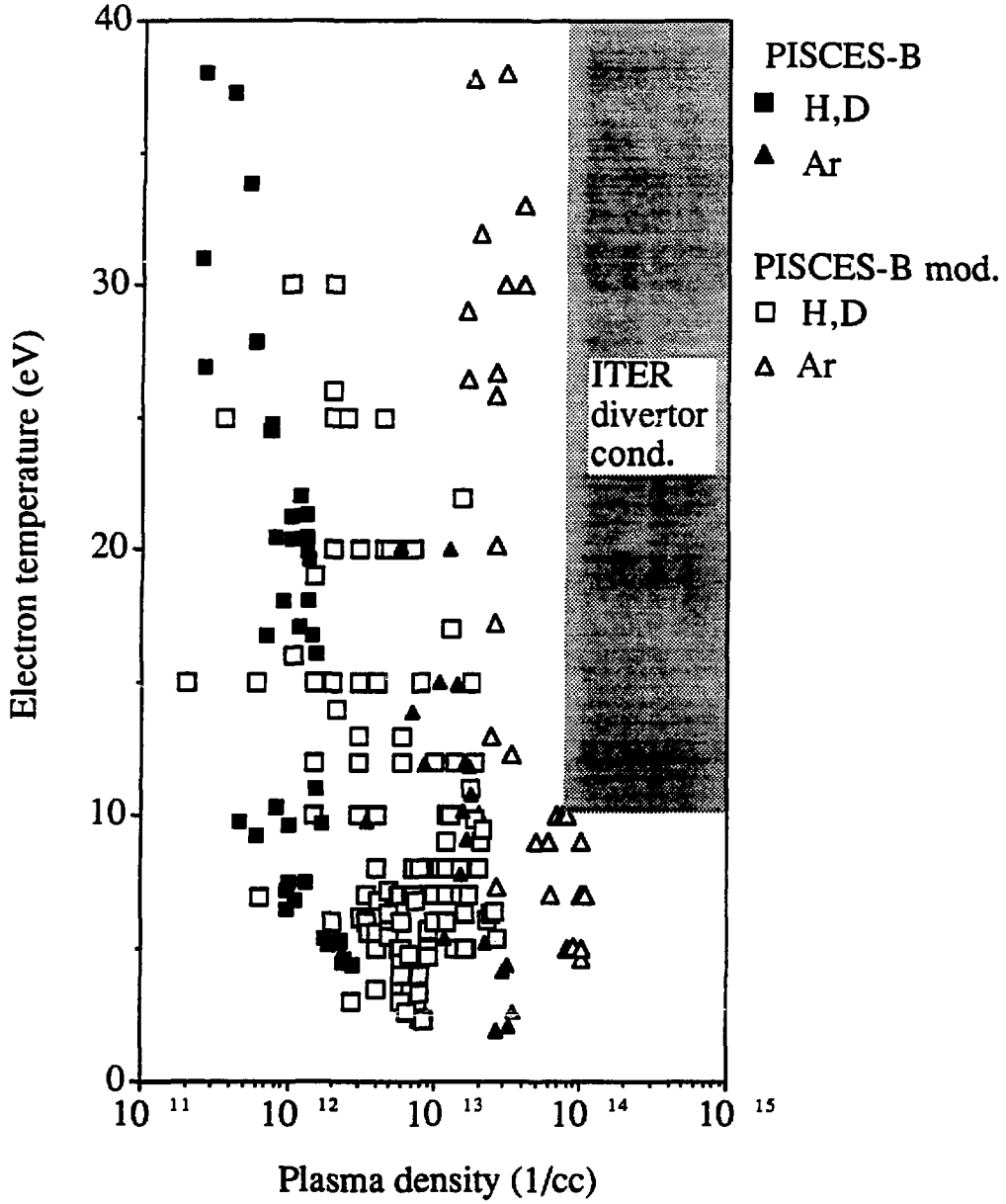

Fig. 2 Improved plasma operation in the PISCES-B Mod. facility.

Table PMI-conditions in PISCES-B Mod. and ITER

PMI-conditions		PISCES-B Mod*.	ITER**
Plasma species		H, D, He Ar, N	D, T, He
Pulse duration (s)		Continuous	200
Plasma density (cm^{-3})		10^{13} (H,D) 10^{14} (Ar)	10^{14} - 10^{15}
Electron temperature (eV)		3-30	10-20
Ion bombading flux (ions s^{-1} cm^{-2})		10^{17} - 10^{19}	10^{19} - 10^{20}
Ion bombarding energy (eV)		30 - 300 (dc bias)	≈ 100
Power load (MW/m^2)		5 - 15 (dc-bias)	30 - 50
PFC (sample) temperature (^oC)		RT - 1700	~ 1000
Ionization mean free path for 1st ionization (cm)	C*** W	~ 1 ~ 0.02	~ 0.5 ~ 0.01
Neutral pressure (Torr)		10^{-3} - 10^{-5}	≈ 10^{-5} for first wall ≈ 10^{-2} for divertor

*PISCES-A can provide similar performance.
**Physics Phase divertor design values from the ITER Conceptual Design: Interim Report.
*** Physically sputtered carbon

PISCES-C Facility: An RF-plasma Facility for Oxygen Plasma Experiments

PISCES-C (Jr.), a plasma-materials interaction facility using an rf plasma source, has recently been upgraded to provide continuously operating, high-density oxygen plasmas. The new setup is shown in Fig. 1. Main features of the upgraded version are:

(1) Vacuum: A wide range of operating pressures (1torr-UHV) has been achieved by using a compound molecular pump with a pumping speed of 1500 liter/sec and a UHV chamber. This provides a wide operating window of plasma parameters and a clean vacuum condition, free from contamination of the diffusion pump oil by oxygen gas.

(2) RF Plasma Source: The antenna is made of copper plates and has the geometry similar to that of the Nagoya-type III. A water-cooling line is soft-soldered on the antenna, so that the temperature and the impedance stay constant during operations. Unloaded quality factor, Q, of the antenna is aimed at around 20 with a power coupling efficiency of 70% and an amplification factor of 60. The impedance of the antenna is matched to 50Ω of the generator by two vacuum capacitors. The tuning capacitor is connected in parallel with the antenna, and the loading is in series with the generator. This setup lowers the required capacitance for matching (1100 pF for tuning and 500 pF for loading).

Plasma is generated inside a pyrex glass tube 25cm long with a diameter of 7cm. The tube has a gas feed-through at the end. Both the capacitors and the tube are air-cooled by a blower at the impedance matching box. The stainless steel cylindrical enclosure surrounding the tube confines the air-flow and connects the matching box to the chamber. To minimize the coupling between the antenna and the enclosure, the enclosure is slotted along the axis. A set of Helmholtz coils provide a magnetic field about 1KG. The magnetic field radially confines the plasma and enables a resonant coupling with helicon waves. This is known to be highly efficient for ionization (almost 100%), thus producing high-density plasmas.

(3) Diagnostics: Due to the fluctuation of floating potential by rf fields, a double probe has been built to measure plasma parameters. To prevent rf pick-up, all the connections are doubly shielded and rf chokes are used. Probe tips are made of tantalum and aligned in parallel with the magnetic field so that the drifting velocity effect can be minimized. Shown in Fig. 2 are the first plasma current data obtained by this probe (for this measurement no magnetic field was applied at the point of the probe). Also, a residual gas analyzer (RGA) is installed to monitor neutral species. This diagnostic makes real-time process monitoring possible for plasma-materials interactions to form volatile species such as: $C + 1/2\ O_2^+ = CO$.

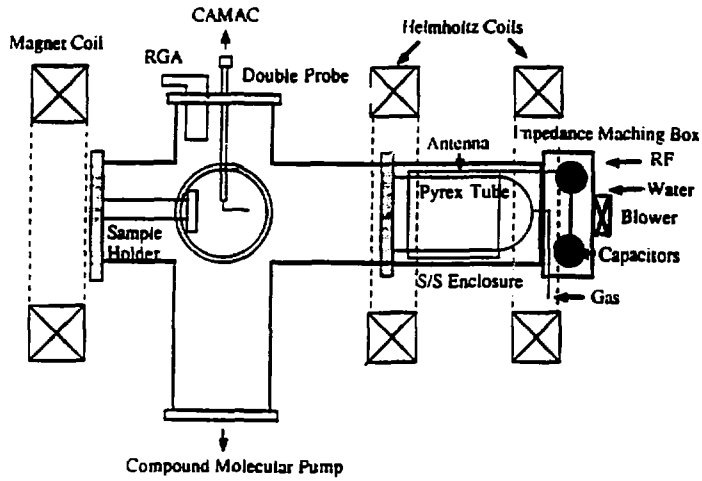

Fig.1 A schematic diagram of the upgraded PISCES-C (Jr.)

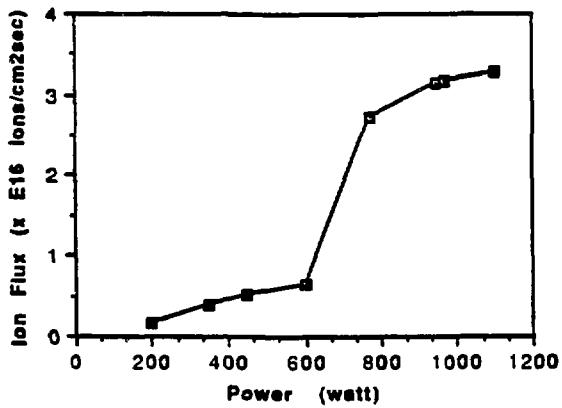

Fig.2 Power dependence of ion flux measured at 28 cm down stream from the source at a pressure of 1mtorr and a magnetic field of 450 gauss

PISCES-Upgrade: A Dedicated Facility for ITER R&D on PFCs

The PISCES-Upgrade (will be referred to as PU) facility has been under design to meet the needs specified in the latest ITER R&D documents for a divertor plasma simulation facility. In particular, this facility can address the erosion/redeposition issue, specifically called out by the ITER team. The PU facility is currently designed to employ a reflex-arc discharge using lanthanum hexaboride (LaB_6) cathodes in an arrangement where the source zone is a magnetic cusp and the uniform magnetic field is 3 kG. The PU facility produces plasmas with a 176 cm^2 cross-sectional area and can fully expose component surface areas up to 350 cm^2. The PU plasma is expected to have a density of the order of 10^{20} m^{-3}, an electron temperature of 5-20 eV, a normal plasma heat flux of 35 MW/m^2 at a -250V bias on the component test assembly, and a corresponding ion flux in the range of 4-8 x 10^{23} $m^{-2}s^{-1}$. Components for testing can be arranged at angles to the incident B-field, and the facility will operate "steady-state".

All the PISCES-A and B devices are basically high-density, continuously operating plasma generators coupled by a magnetic field to a materials interaction region. The species of the plasma flowing into the interaction region is determined by the gas fed into the plasma generator. The ion temperature in PISCES-A and B is about a few electron volts. Therefore, if a dc bias is applied to the target, the incidence of ions is approximately normal to the surface. The electron temperature and density in PISCES can be controlled by appropriate adjustment of the discharge power, gas feed rate, and magnetic field strength. The PU facility design is based upon the operating experiences obtained in PISCES-A and PISCES-B.

The optimum geometry for high-density plasma generation comprises a short radial diffusion length coupled with a low magnetic field in the anode region. Inherent in the magnetic cusp geometry is a short anode-cathode radial separation, a large area plasma at the target location, and a region of lower magnetic field strength in the region of the anode. In a single cusp source arrangement, a magnetic cusp is formed between two large coils, and the magnetic field lines from the cusp are connected to the component test region by a long solenoid (see figure).

In addition, RF heating of ions up to energies ranging 10-20 eV is under consideration to make the plasma impact power to the target more relevant to that expected in ITER. Hot ions will make non-normal incidence of ions to the target, which can lead to a critical difference in the target sputtering behavior. Also, the application of superconducting magnets is currently evaluated.

PISCES-Upgrade Cusp Source Geometry

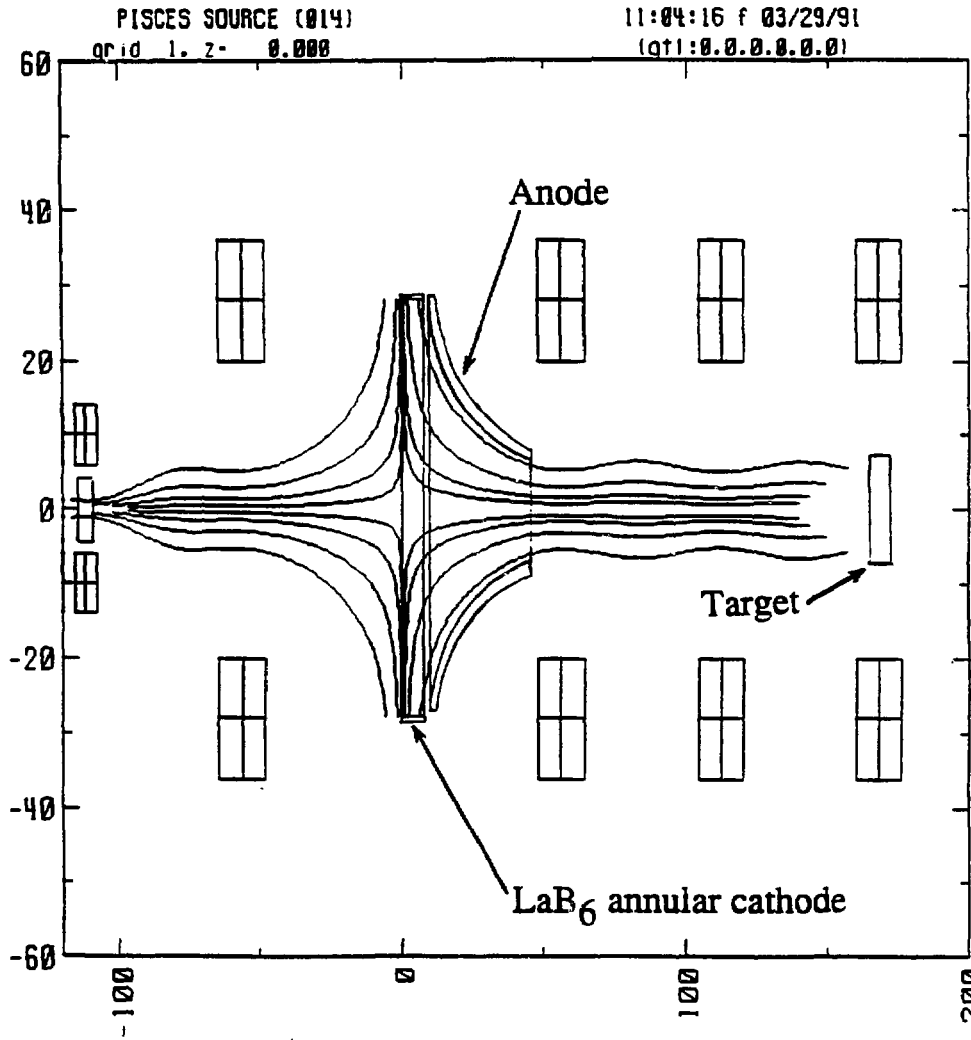

Figure 1 - Source and magnetic field geometry for PISCES-Upgrade.

SEM-EDX Facilities (UCLA-TRW Laboratory)

Materials for plasma-facing components like boronized graphite and C-C composites are being routinely analyzed in the PISCES laboratory using Scanning Electron Microscopy (SEM) using the JEOL T-330A, and Energy Dispersive X-ray Analysis (EDX) using the KEVEX DELTA CLASS IV system.

The boron Kα line at 0.185 keV is very difficult to detect because it has a very low excitation probability and, at the same time, a very high probability of being absorbed in the sample matrix on emission[1]. Also, the B Kα line lies at the edge of the electronic noise of the Kevex X-ray detector so that a part of the peak is lost in the noise. Further, in case of boronized graphite, the B Kα (0.185 keV) and C Kα (0.282 keV) peaks overlap since the FWHM for the Kevex system is 160 eV. With these limitations, the system has been optimized to detect boron from boronized graphite having a boron concentration greater than 3%.

Using pure boron (99.9%, Cerac), pure Graphite (POCO) and B_4C as reference materials, the calibration curve has been obtained for boron concentration in boronized graphites as shown in figure 1. The offset seen for 0% B arises due to the B and C peak overlap in the EDX spectra.

For standard based analysis, a Faraday cup is used to measure the electron beam current. Analysis is done using the deconvolution technique [1] so as to account for the distortion of the boron peak due to the electronic noise. The Kevex Quantex software is used to apply ZAF corrections to the 'k' ratios* obtained using reference deconvolution, and determine the percent atomic as well as weight concentration of B in boronised graphite. Figure 2 shows the analysis results for a number of samples using the standard based technique. The scatter in the data is probably due to variation in the boron concentration from sample to sample.

Another important feature of the Kevex EDX system is the availability of X-ray mapping, i.e. the areas of the sample where boron is concentrated can be determined. This feature is especially useful for the analysis of two-phase materials such as boronized graphites. A comparative study of EDX and other techniques such as AES and ESCA is being conducted [2] on the analysis of boronized graphites and carbon-carbon composites.

---

* 'k' ratio is the ratio of the peak intensity of the sample to the peak intensity of the reference standard.

[1] 'Kevex Quantex Software Reference Manual.' Kevex Instruments 1985.
[2] M.Khandagle, to be published in Surface Science.

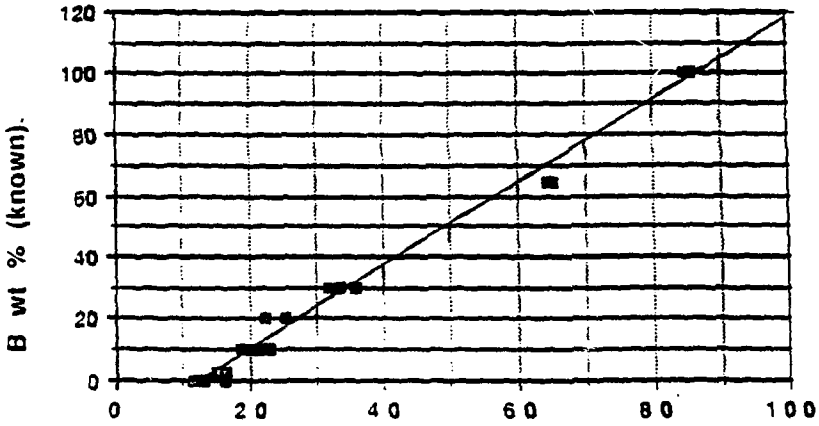

B (known) = - 16.662 + 1.3397 B (dec/int).

Figure 1: Calibration curve for Boron by dec/int.

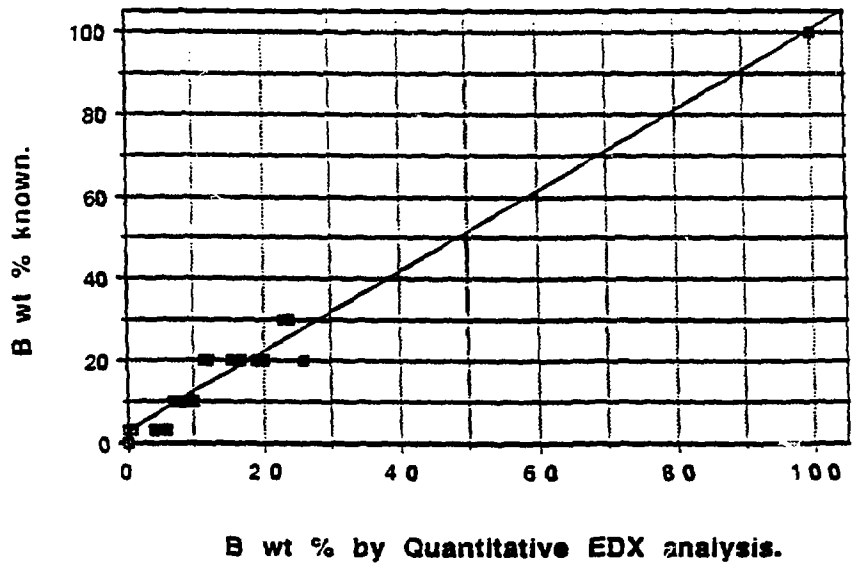

Figure 2: Results for B concentration by quantitative EDX analysis.

Fast Scanning Probes as Diagnostics for Steady-State Plasmas[1]

The fast scanning probe developed by the PISCES-team uses a pneumatic cylinder to drive a combination emissive and mach probe tip across the plasma column. This allows for single scan or shot profiles of the space or floating potential, density, and parallel mach number. Profiles of the space and floating potentials under identical plasma conditions can be obtained by using successive shots of the fast probe. To record the floating potential profile, the emissive probe tip is left cold. To record the space potential profile, the probe is resistively heated so that it will thermionically emit electrons into the plasma.

A schematic diagram of the probe structure is shown in Fig. 1. The fast probe actuator has a 15cm stroke and the total round trip time for the probe is 300 msec. The probe is constructed of an alumina shaft with six holes for wires to pass through. The tip is made up of five electrical probes: a loop of thoriated tungsten wire for the emissive probe, and two pairs of unidirectional probes. Each pair of unidirectional probes has one tip that faces towards the source ("upstream") and the other faces away from the source ("downstream"). One pair has tips larger than the ion Larmor radius and is referred to as a magnetized mach probe, while the other pair is smaller than the ion Larmor radius and has been used to study ion flow in plasma wakes. The parallel mach number is computed from the ratio of the currents collected by the upstream and downstream magnetized probes. Density profiles are computed from the average of the current collected by the two probes.

The fast probe diagnostic was first built for the PISCES-A facility and has been used for virtually all the edge-plasma physics experiments including: presheath profile measurements in front of material samples, the modification of the potential profiles and scrape-off layer lengths in biased scrape-off layer simulation experiments, ion flows in the wakes of probes in the plasma, modification of density profiles in RF limiter/divertor simulation experiments.

Also, a fast scanning double probe has been built for materials experiments in the PISCES-B facility. During the fast probe stroke, the probe tip voltage will be swept rapidly. This results in a number of Langmuir probe traces at different radii. These traces can be fitted automatically by the data acquisition system to produce a discrete spatial profile of electron temperature and density across the plasma column. Also, the use of the fast probe in PISCES-B material experiments will minimize sample contamination resulting from sputtered probe materials. This is important because under plasma bombardment the surface modification can readily be triggered by trace amount of impurities [2].

[1] R. Lehmer et al., UCLA-Report# UCLA-PPG-1228 (1989).
[2] Y.Hirooka et al., Nucl. Instr. & Methods-B 23(1987)458.

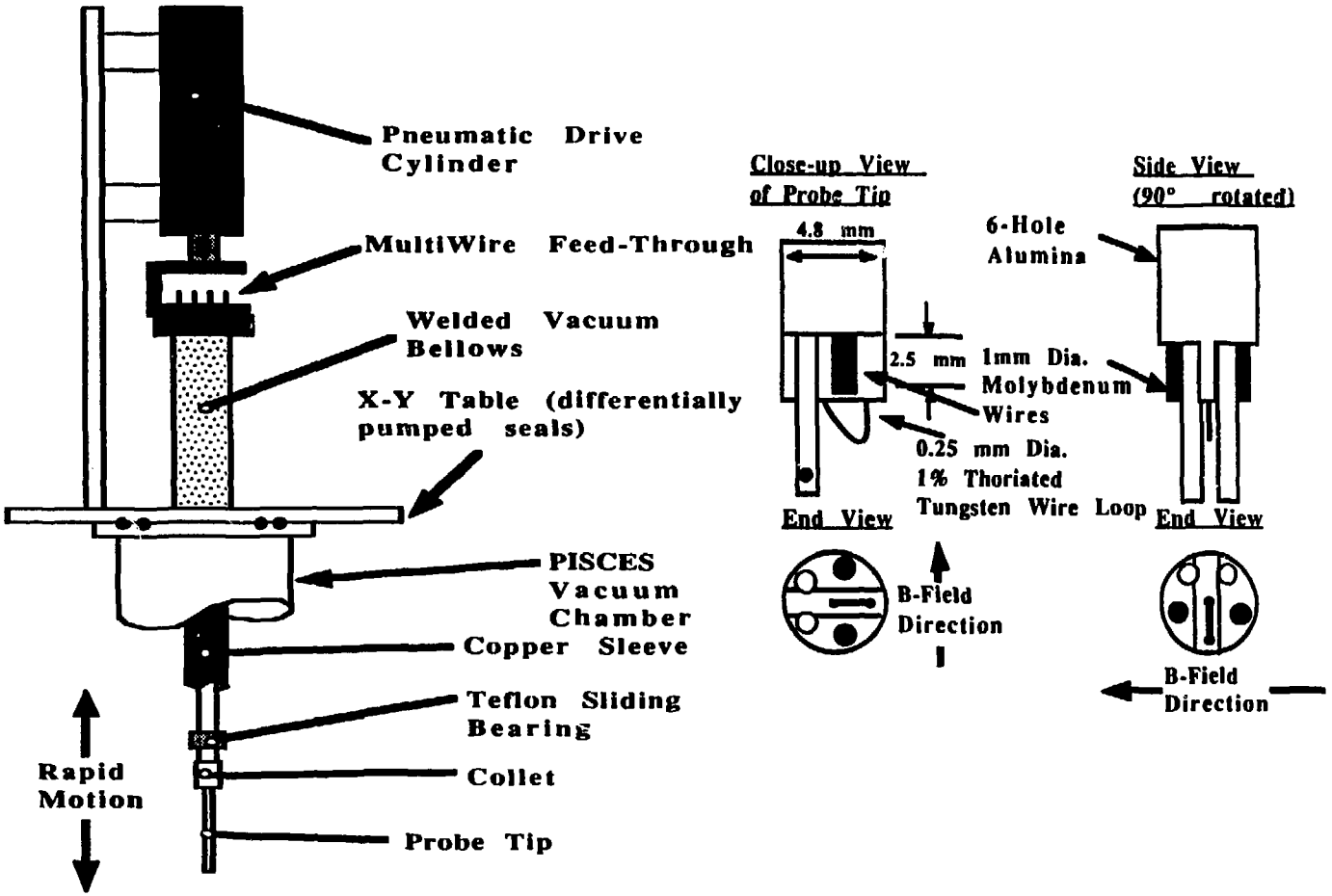

Fig. 1 A schematic diagram of the fast-injection probe.

Spectroscopic diagnostics for PISCES A, B and C(Jr.) Facilities

Spectroscopic techniques have been applied in the PISCES A, B and C (Jr.) facilities in diagnosis of material erosion yields [1], surface temperature profile [1], hydrogen recycling [2], impurities[3], neutral and ion temperatures and densities [4] and chemically reactive RF plasmas [5]. In addition to its uniqueness as an in-situ erosion yield measurement in material experiments, spectroscopic techniques have emerged as an integral part of plasma physics experiments.

Spectroscopic diagnostic instruments available in the PISCES Laboratory include a 1.3M Czerney-Turner spectrometer, a 0.5M Crossed Czerney-Turner spectrometer, an OMA (Optical Multi-channel Analyzer) system, a CID camera with a computer image analysis system. Also, a 0.3 M Crossed Czerney-Turner VUV spectrometer has recently been installed on the PISCES-B facility.

As to applications of these instruments, for example, OMA can be used along with spectrometers to obtained both spectral and spatial information of plasma impurities. The CID camera can be used to obtain spatial emission profiles or can produce spectral and spatial profiles simultaneously when integrated with the spectrometers. These arrangements have been made possible by efforts in the laboratory to bridge between separate instruments with customized computer software.

Because of its applicable wavelength range (between 105nm and 60 micrometers), VUV is particularly suited to study materials containing carbon and/or boron such as boronized graphites and C-C composites (see Fig. 1). The OMA system is integrated with this spectrometer to obtain emission lines of carbon and boron on the same spectra allowing direct comparison between these elements (see figure 1).

In addition to these instruments, a 10 m Å limit resolution Fabry-Prot interferometer has recently been installed on the PISCES-A facility. This interferometer is currently used in conjunction with spectrometers to increase resolution. Using the improved resolution, direct spectroscopic measurements are planned to analyze the neutral temperature in argon plasmas in PISCES-A.

[1] Y.Hirooka et.al. Fusion Technol. 19(1991)2059.
[2] R.Doerner et.al. J.Nucl.Mater. 176&177(1990)954.
[3] W.K.Leung et. al. Bull. Am.Phy.Soc. 31 (1986)
[4] L.Schmitz et. al. J.Nucl. Mater. 176&177(1990)522.

Fig. 1 Emission spectra from DMA

Vacuum Outgassing Facility for Thermal Desorption Spectrometry [1]

It is widely recognized that outgassing from plasma-facing components in tokamaks can significantly affect the performance of plasma confinement. Therefore, it is of considerable importance to study the outgassing behavior of materials using off-line facilities. The thermal desorption spectrometry (TDS) technique is widely used to measure outgassing characteristics of materials.

To perform outgassing measurements a dedicated UHV system was constructed first in 1988 and then upgraded in 1990. A schematic diagram of this outgassing facility is shown in Fig. 1. Major components are: (1) 6-way cross stainless steel chamber; (2) BA-gauge; (3) a turbomolecular pump with a pumping speed of 170 l/s; (4) a residual gas analyzer (RGA) with a PC-data acquisition system; and (5) a computer-controlled infrared (IR) furnace.

In this outgassing facility, a test sample can be heated by the IR-furnace from room temperature to temperatures around 1000°C typically at a rate of around 20 deg/min. During the course of thermal desorption measurement, partial pressures of desorbed gases are monitored with the RGA system.

As an example, the thermal desorption spectra from a bulk-titanized graphite sample are shown in Fig. 2. The total amount of desorbed gasses is calculated from the time-integration of their partial pressures. In this case, the total amount of gas desorption is evaluated to be 2.64×10^{18} molecules/cm^2. Also, this system has been used for evaluating deuterium retention in bulk-boronized graphites after plasma bombardment [1].

From these TDS data, the activation energy (E_d) for the desorption process can be estimated using the relation [2]:

$$(E_d/RT_m^2) = (\nu_d \, n \, \sigma^{n-1}/\beta) \exp(-E_d/RT_m) \qquad (1)$$

where n is the order of the surface reaction, T is the peak temperature, ν_d is the frequency factor, σ is the concentration of the gas, β is the temperature ramp rate.

As part of ITER-R&D effort, erosion-redeposition experiments have recently been conducted on high-Z materials such as tungsten. It is planned that the activation energy for the desorption of deuterium from selected high-Z materials is evaluated using eq.(I).

---

[1] Y.Hirooka et.al. Fusion Technol. 19(1991)2059.

[2] P.A.Redhead Vacuum 12 (1962) 203

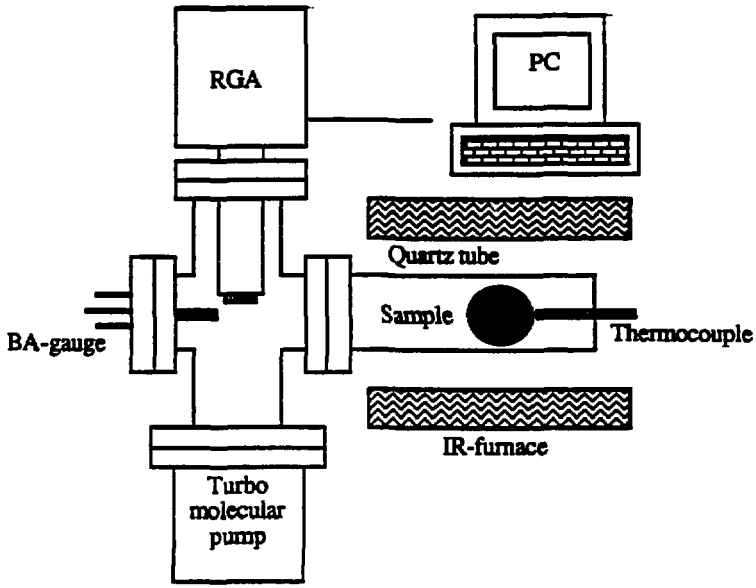

Fig. 1 A schematic diagram of the vacuum outgassing facility.

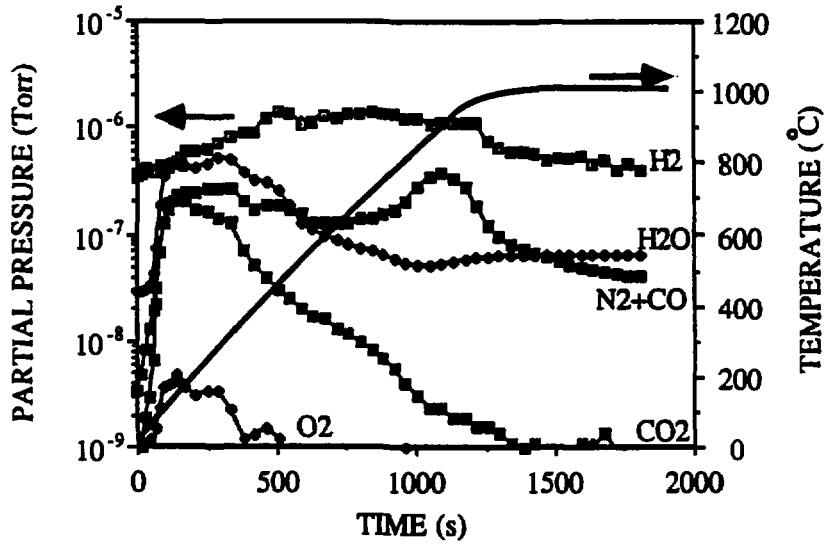

Fig. 2 Desorption from titanized C-C composite (CCTK-420).

Computer Data Acquisition System in the PISCES Laboratory

The PISCES data acquisition system provides for the acquisition, storage and manipulation of raw and processed data from the PISCES-A, PISCES-B and CCT Tokamak. The main components of this PISCES Data Acquisition system are the CAMAC(Computer Automated Measurement and Control) crates containing fast and slow data loggers which are connected to a VAX cluster,consisting of 2 Micro Vax-II, 2 DEC 3100/76(with RGB color monitors) and three VAX 2000 workstations (Fig.1). A Serial Highway Driver is attached to the VAX cluster which establishes the communication with CAMAC crates through the Fiber Optics cables, providing high voltage isolation from the PISCES and TOKOMAK machines.

The CAMAC crate connected to the pisces-A machines contains two 32-channel slow loggers and is capable of sampling data at a rate of up to 100 KHZ.The number of active inputs is programmable.To achieve maximum sampling rate fewer inputs are used depending upon the available memory in the crates.Individual channels have descriptive logical names assigned to them which facilitates user access to the raw and processed data. ORNL CAMAC crates drivers are used for setting up the data loggers and acquisition of the raw data from the CAMAC crates.

Recently the Hythech Ethernet CAMAC module was successfully tested in PISCES facilities. The significance of this new CAMAC module is that it eliminates the need for CAMAC Serial Highway and with this system the acquisition of data is done through the Ethernet and then the data is transmitted to the target Workstations.

The VMS operating system has been upgraded to 5.4 ,in this upgrade all window system and the Graphics Users Interfaces also upgraded to X-window system (DEC-windows).PISCES developed the prototype graphics interfaces in this X-Window system so the 3100 workstation could become functional for the research staff.

The DACP (Data Acquisition control programs) have also been upgraded so that they can become operational in this new DecWindow environment.DACP controls the continuous as well as post-triggered data sampling on PISCES-A and PISCES-B machines. The DACPs provide the users controlled data acquisition functions and also compute the processed data from the recently retrieved raw data.The CAMAC crate used by the CCT Tokomak contains two fast loggers each with 4 channels capable of sampling data at 1 MHz and one slow logger with 32 channels.

The MIT MDS software provides the database facilities for the VAX cluster environment which enables the structured storage of Raw, Processed and Compressed data. Apart from this,other customized software using IDL,PVI-DI and DISSPLA graphics packages provide the realtime data analysis and manipulation capability. In addition, PISCES developed the Double Probe analysis code for analyzing the data from the fast probe on PISCESB machines. Further improvements and refinements have been included in this software so it can be used at other sites(DIII-D,PBX).

The VAX cluster is connected through an ETHERNET to a DecServer200 terminal server connecting other varieties of peripherals(4 Macintoshes,2 IBM PC/AT XT,TEK-4015, TEK 4696 for color graphics capabilities,modems for communications,and DEC Laser printer for hard copies). Terminal emulation programs executing on the Macintoshes and IBM PC facilitate transfer of data to and from the VAX Cluster environment. The PISCES CLUSTER is also connected to the Fusion Research Academic network VAX-8350(FRAN), which provides the network capabilities to other networks, such as MFENET (Magnetic Energy Fusion Network) and ESNET(Energy Science Network).

Also, 2 DEC 5000/200 workstations have recently been added, which will be used primarily for 3-D CAD, CAM applications (w:. PRO-ENGINEER). These workstations are in RISC platforms with Turbo Graphics Accelerator which provides high speed graphics emulation as well as realtime computation. Currently, MATHMATICA application has been installed on one of the DEC 5000 workstations and it has been used by the research staff for data analysis and simulations.

FIGURE - 1

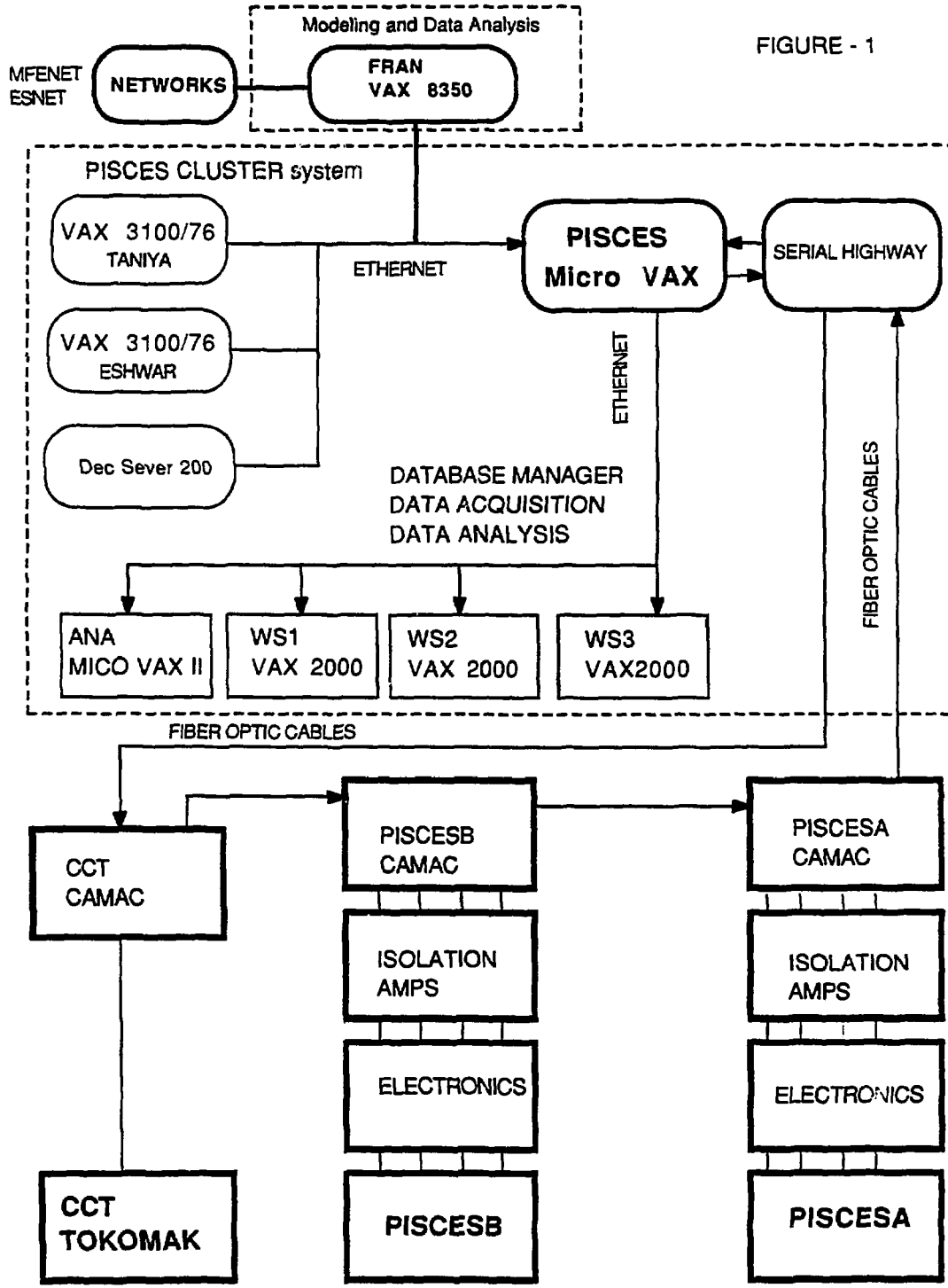
Modeling and Data Analysis
MFENET
ESNET
NETWORKS
FRAN
VAX 8350
PISCES CLUSTER system
VAX 3100/76
TANIYA
VAX 3100/76
ESHWAR
Dec Sever 200
ETHERNET
PISCES
Micro VAX
SERIAL HIGHWAY
ETHERNET
DATABASE MANAGER
DATA ACQUISITION
DATA ANALYSIS
FIBER OPTIC CABLES
ANA
MICO VAX II
WS1
VAX 2000
WS2
VAX 2000
WS3
VAX2000
FIBER OPTIC CABLES
CCT
CAMAC
PISCESB
CAMAC
PISCESA
CAMAC
ISOLATION
AMPS
ISOLATION
AMPS
ELECTRONICS
ELECTRONICS
CCT
TOKOMAK
PISCESB
PISCESA

3. PISCES Experiments

-Materials and Surface Physics-

Evaluation of Tungsten as a Plasma-Facing Material for ITER

About a decade ago, there was a vital discussion whether low-Z materials such as carbon are better than high-Z materials such as tungsten in use for plasma-facing components (PFC) in fusion devices. Before this discussion became conclusive, low-Z PFCs were installed in major tokamaks such as TFTR, JET and JT-60, and have improved plasma performance, relative to Med.-Z PFCs. However, the successful application of low-Z PFCs in the presently operating devices has resulted in a temporary but worldwide slowdown of high-Z materials research and development for fusion applications.

In fact, low-Z materials are currently planned to be used for the divertor plate in ITER in the Physics Phase where the "ignition" is the main objective. However, in the Technology Phase where long-pulse burning is intended the requirements for PFCs are much more difficult to be met. Attention has recently been paid to estimating the lifetime of the divertor plate in the technology phase of ITER. Regarding lifetime, tungsten is more practical than graphite because of its high threshold energies for physical sputtering (calculated values of $E_{th.}$ for W are 783, 341, 213 eV for H, D, T, respectively [1]). This means that if the edge plasma temperature is controlled around few tens of electron volts, one can in principle eliminate sputtering of the tungsten divertor plate due to fuel particles.

In this work, tungsten and its coatings on molybdenum are evaluated with respect to erosion and gas retention under steady-state deuterium plasma bombardment in the PISCES-B facility [2]. Plasma bombardment has been conducted at ion bombarding energies below 500 eV, ion fluxes above 10^{18} ions s^{-1} cm^{-2}, electron temperatures around 15 eV and surface temperatures above 1000°C. The probability of redeposition is calculated to be about 10%, using the WBC Monte Carlo code [3]. Therefore, erosion yield data obtained here can directly be compared with classical sputtering yield data.

Both the weight loss and in-situ spectroscopy [4] methods have been used to evaluate the erosion yield of tungsten. Data indicate that tungsten erosion starts at energies around 100 eV, significantly lower than the theoretical threshold energy. Tungsten coatings prepared by a halogen CVD process have shown similar erosion behavior to bulk-tungsten. Thermal desorption was conducted for plasma bombarded tungsten at 500 eV at 1300°C. The total amount of deuterium retained is found to be about 7×10^{15} D-atoms/cm^2, nearly two orders of magnitude below the corresponding value for graphite.

[1] N.Matsunami et al. Atom.Data & Nucl. Data Tables 31(1984)1.
[2] Y.Hirooka et al. J.Vac.Sci. & Technol. A8, 1790 (1990).
[3] J.N.Brooks, Phys. Fluids. B2(8) (1990)1858.
[4] Y.Hirooka, et al. J.Vac.Sci.&Technol. A7(1989)1070.

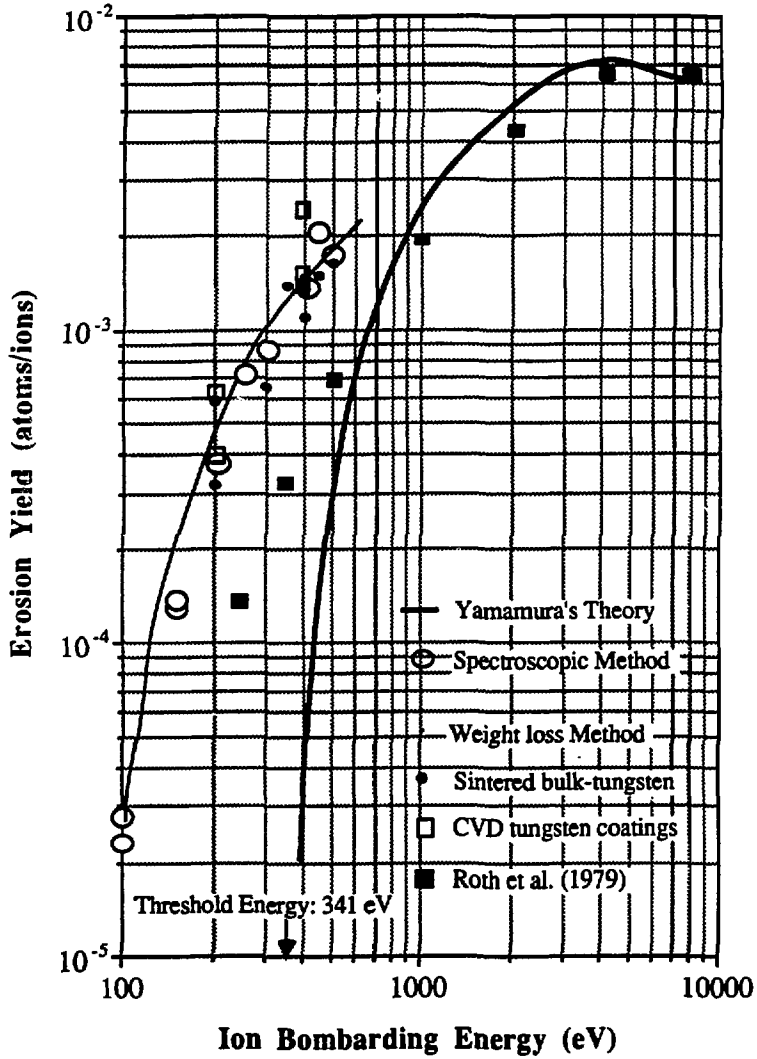

Fig. 1 Erosion of tungsten due to deuterium plasma bombardment at 1500 deg. C in PISCES-B. Notice that experimental data indicate erosion starting at an energy much lower than the calculated threshold energy for physical sputtering.

Solid Target Boronization using Boronized C-C composites

Boronization has been used for wall conditioning in many magnetic fusion devices and has resulted in noticeable improvement of plasma confinement. However, the conventional boronization technique requires the use of large amounts of hazardous (explosive or toxic) gases such as di-borane, B_2H_6 or boron tri-methyl, $B_2(CH_3)_3$ as the source of boron. Therefore, special facilities have to be built in to handle these gases. For safety and convenience, gas boronization has been implemented in most devices over the weekend.

In addition to these boron-containing gases, methane CH_4 is often fed in the gas boronization process so that the coatings consist of boron and carbon, presumably forming boron carbide in the coatings. Because hydrogen is a major constituent of these feed gases, a fair amount of hydrogen is unavoidably incorporated in the coatings. This makes gas-boronized walls act as a source of hydrogen extraneous to plasma discharge, leading to a great difficulty controlling plasma density during confinement experiments. Therefore, as a second stage of wall conditioning, helium glow discharges are employed to remove hydrogen from gas-boronized walls. However, together with hydrogen boron is also removed due to sputtering. Furthermore, boron will be eroded during confinement experiments even more severely. Obviously, the effect of gas-boronization has a finite lifetime, not compatible with long-pulse fusion experiments.

A new boronization technique has been developed to overcome these difficulties. This technique is called Solid Target Boronization (STB). In the STB technique, instead of hazardous gases a boron-containing solid is used as the boron source. Exclusively for the demonstration of STB, UCLA and Toyo Tanso jointly developed a new boronized carbon-carbon (C-C) composite material which meets the thermal shock resistance and low-Z requirements for this application. The first application experiment of STB was done in the Tokamak de Varennes (TdeV) as part of the US-Canada collaboration.

The boronized C-C composite was machined into a mushroom shape with a diameter of 7 cm and was mounted on a sample manipulator in TdeV. (From separate experiments, it is known that the mushroom in this dimension is not large enough to "limit" the plasma.) The boronized target was exposed directly to confinement plasmas at positions typically 1-2 cm beyond the last-closed-flux-surface (LCFS) determined by two main graphite limiters.

For the STB experiment, first about 100 limiter discharges and then about 100 double-null divertor discharges were made. Selected plasma discharge parameters from limiter experiments are shown in Fig. 1. In this figure, two cases with/without STB are

loop voltage decreases by about 40% (Fig. 1-(c)). Visible bremsstrahlung decreases by about 60% (Figs. 1-(d)). Consistent with these findings, a significant decrease in O-II radiation, relative to nitrogen as the reference, is observed as shown in Fig. 2. Also, soft X-ray measurements indicate a reduction of radiation due to metallic impurities such as Fe, Cr, and Ni. These data prove that the STB technique is effective in reducing impurity radiation and hence improving plasma performance. Similar results were obtained for divertor-plasma experiments.

For a typical limiter shot, the surface temperature was optically measured to be around 2000°C or even higher towards the end of a flat-top. Therefore, the emission of boron from the target is considered to be driven strongly by evaporation in addition to sputtering (RES). Also, thermionic electron emission becomes substantial at temperatures around 2000°C. Consistent with this thermionic emission property, the floating potential of the target becomes positive towards the end of a discharge (Fig. 1-(e)).

The gas puffing rate, feedback-controlled with the plasma density, increases by about a factor of about 3 (Fig. 1-(f)). No significant change in edge density and electron temperature has been observed during STB. Thus, it is assumed that the fueling efficiency remains unchanged. Also, the neutral pressure in the torus tends to decrease when STB becomes effective. Therefore, the increase in gas puffing rate is interpreted as a sign of codeposition of hydrogen with carbon and boron. This means that torus walls with STB act as a sink to hydrogen. The reduction of metallic impurity radiation is due to the coverage of codeposits on portions of the wall, not protected by graphite tiles.

After tokamak-exposure the boronized C-C target shows no macroscopic cracks, but plasma footprints in gray. Interestingly, the gray area is found to be significantly depleted of boron. A silicon deposition probe in TdeV is redeposited with materials to a thickness of about 300-400 Å after 200 discharges for STB. As shown in Fig. 3, Auger analysis indicates that for a wide range of thicknesses, a typical composition is about 10% oxygen, 50-60% carbon and 20-30% boron. ERD (Elastic Recoil Detection) analysis has shown that hydrogen with a concentration of 7×10^{17} atoms/cm^2 is incorporated in these redeposits. This again support the codeposition argument.

In summary, the STB technique has proven to have critical advantages over the conventional gas boronization technique. These advantages include: (1) high safety factor for handling of boron source materials; (2) low cost of the facility needed for boronization; (3) no finite lifetime for the gettering effect (self-reconstructive coatings); and (4) ease of density control (co-deposition effect to pump hydrogen).

[1] Y.Hirooka et al., to be published in Nucl.Fusion.

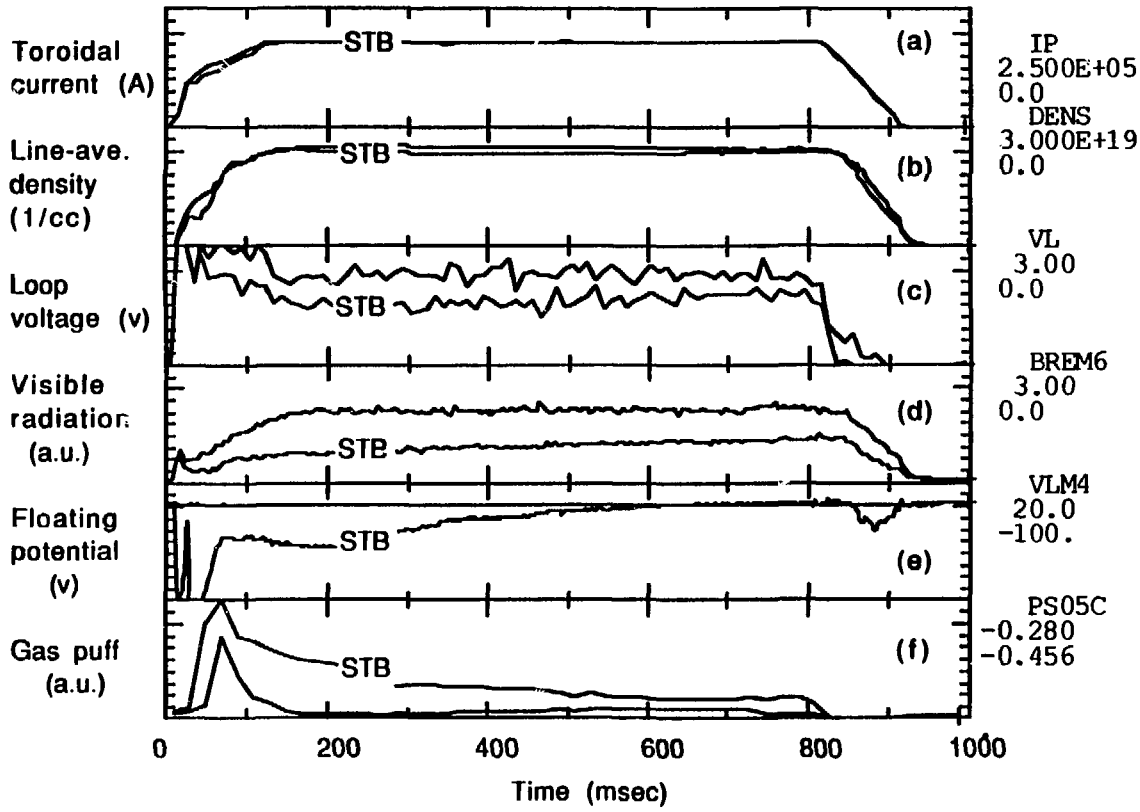

Fig. 1 Effects of solid target boronization on plasma parameters in TdeV.

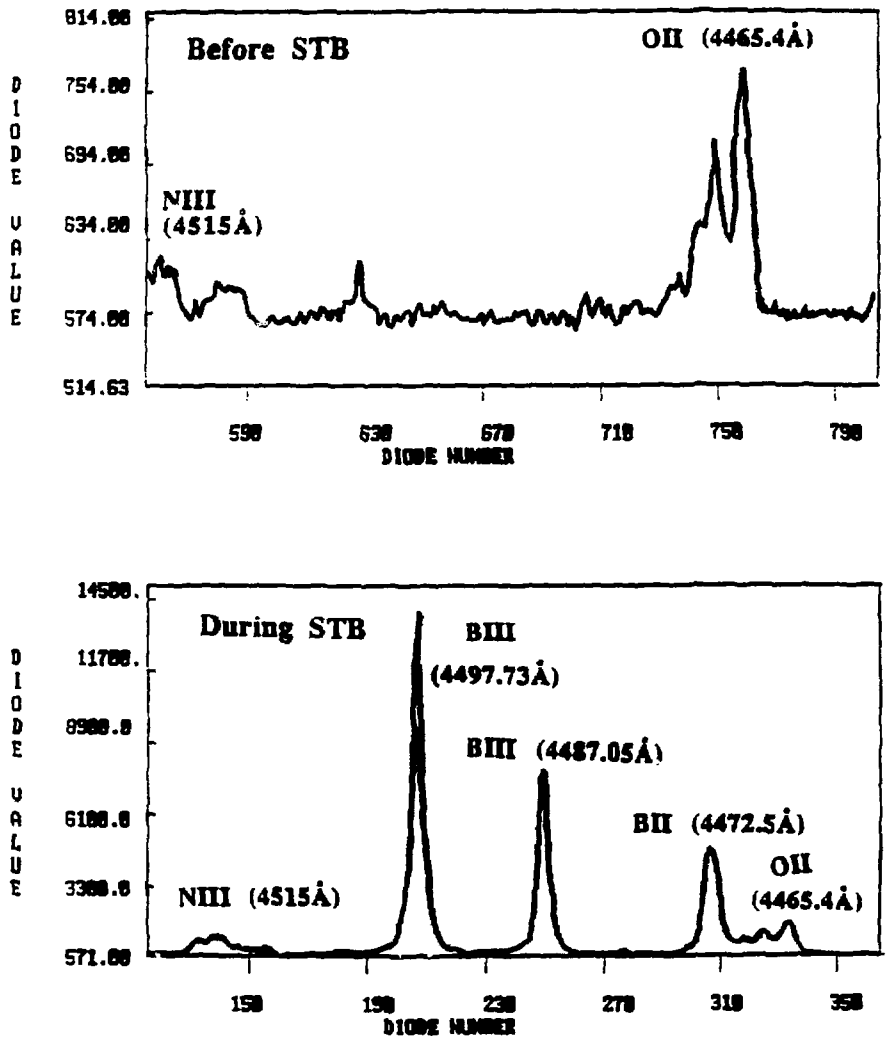

Fig. 2 Spectroscopic measurements for oxygen, boron and nitrogen (as the reference) before and during STB. Notice that the O-II peak reduces significantly with STB.

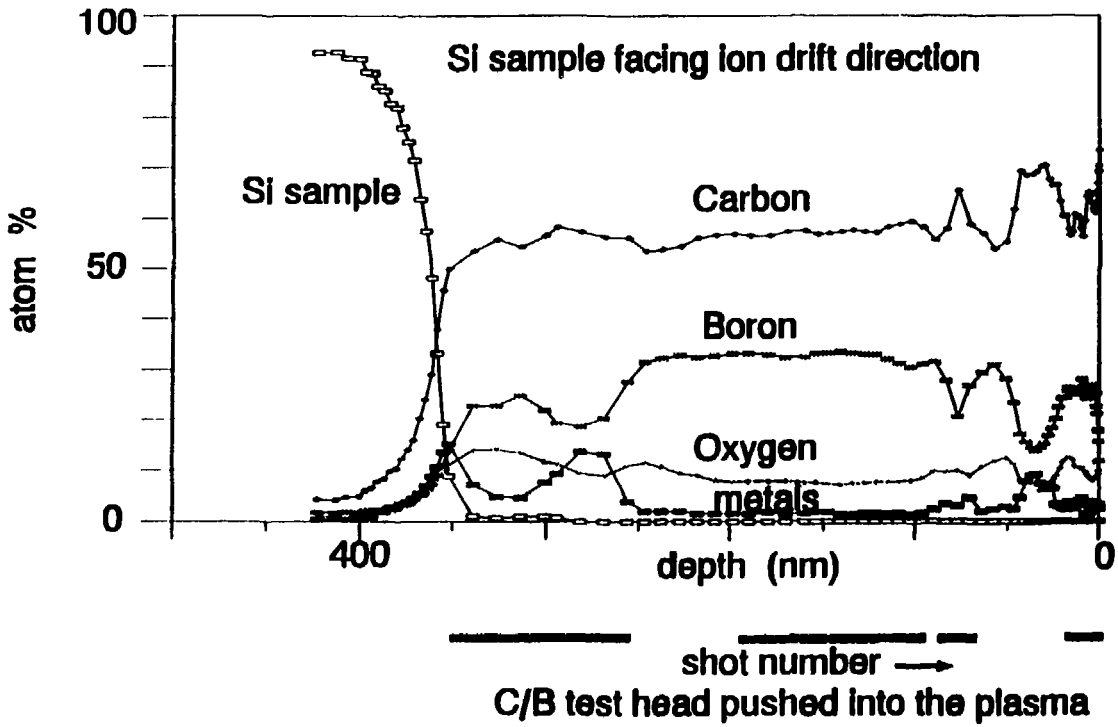

Fig. 3 AES depth profile analysis of a Si deposition probe, facing the ion side, in TdeV after about 200 discharges for STB experiments.

Bulk-Boronized Graphite Limiter in the Wendelstein VII-AS Stellarator

Over the last few years the PISCES-team at UCLA and Toyo Tanso Co.Ltd., Japan have worked jointly to develop a new material, bulk-boronized graphite with a boron concentration from 3-30%, for plasma facing component applications. The evaluation of bulk-boronized graphite was done in collaboration with other institutions, covering major technology issues related to ITER-R&D on plasma-facing components. These issues include: (1) plasma erosion (UCLA); (2) outgassing (UCLA+Toyo Tanso) (3) T-inventory (SNLL); (4) thermal shock resistance (SNLA); and (5) oxidation resistance (Toyo Tanso+INEL). Data from these laboratory experiments indicate that bulk-boronized graphite is clearly superior or equivalent to ordinary graphite [1]. Also, 10% bulk-boronized graphite was tested in the Tokamak de Varennes as the mushroom limiter material and successfully demonstrated reduced erosion, relative to ordinary graphite [2].

Based on these data, it has been decided to use 20% bulk-boronized graphite for the limiter in the Wendelstein VII-AS Stellarator (W-7AS) at IPP-Garching. In this device, titanium carbide coatings were used for the limiter and thus titanium was the main impurity in confinement discharges even after gas-boronization. The application of bulk-boronized graphite was primarily intended to reduce (eliminate) titanium radiation. It is also hoped that if boron is sputtered from the limiter and sprayed over the first wall, then one may be able to see boronization effects similar to those seen with STB.

The first wall conditioning experiments were done jointly by IPP and UCLA-teams. About 300 helium discharges were made for conditioning the new limiter material. The plasma heating was done by ECH with a power input of about 250 kW. The central helium plasma density ranges from 10^{13} to 10^{14} 1/cc.

Generally, bulk-boronized graphite needs to be outgassed at high temperatures (about 1000 ^{o}C) prior to the use in vacuum. However, the baking temperature for W-7AS is only 120 ^{o}C, and therefore a fair amount of gases, mainly hydrogen, is expected to be released during helium conditioning discharges either by thermal desorption or by ion-impact desorption mechanisms. Under these circumstances, one can consider the H_α intensity as the measure of surface conditioning. Fig. 1 shows the H_α intensity during flat-top corrected by input power and plasma density. Notice that the H_α intensity increases towards the end of each day, presumably due to thermal desorption, but decreases day by day. After about three days of helium discharge conditioning, the surface was found to be successfully conditioned and was ready to be used for deuterium discharges.

[1] Y.Hirooka et al. Nucl. Mater. 176&177(1990)473.
[2] Y.Hirooka et al. to be published.

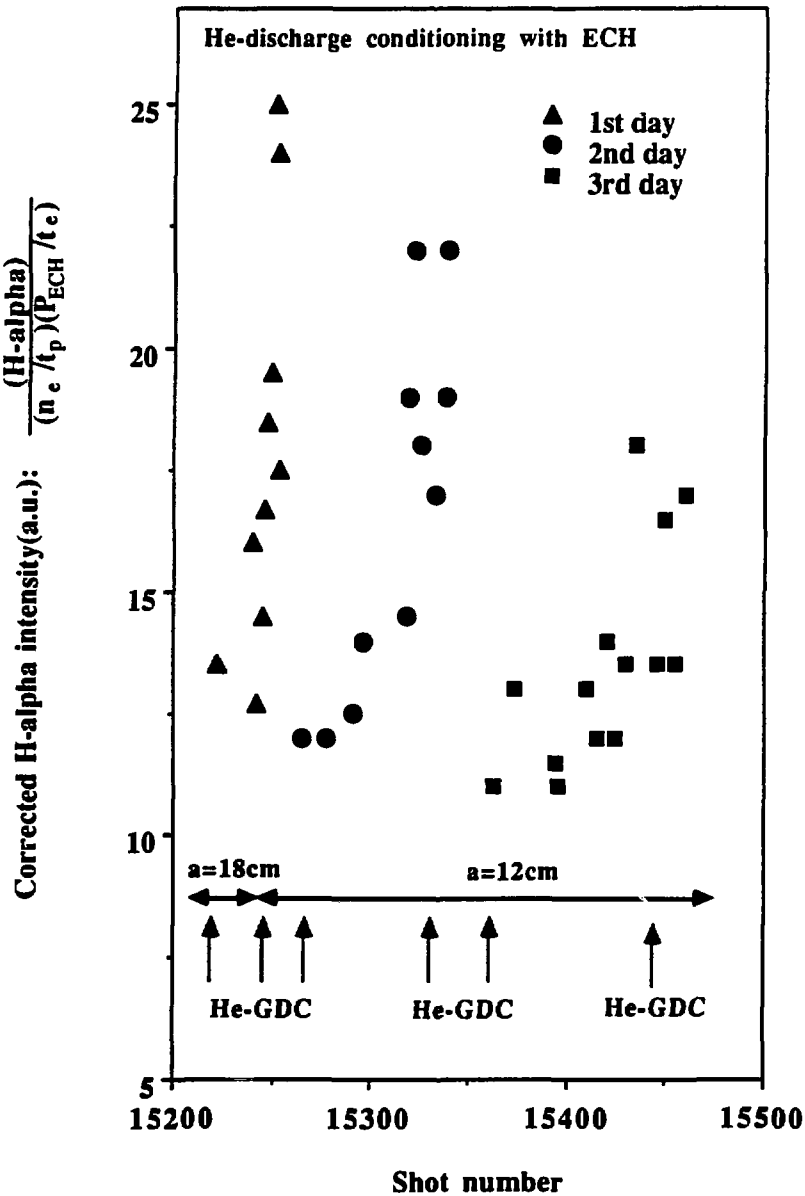

Fig. 1 Corrected H-alpha intensity from the bulk-boronized graphite limiter in the Wendelstein VII-AS stellerator at IPP, Garching. The distance between the top and bottom limiters was set at a=18 cm and a=12 cm.

Impurity Transport Driven by Repeated Erosion and Redeposition

In magnetic fusion devices, materials eroded from surfaces can be ionized due to electron impact, trapped by the magnetic field and then redeposited. In general, the magnetic field is incident on the surface at angles other than normal. As a result, repetition of erosion-redeposition processes leads to a one-way, crossfield transport of eroded materials. It is, therefore, of significant importance to take into account this crossfield transport for the estimation of the lifetime of plasma-facing components. This is particularly important for long-pulse and/or steady-state fusion reactor such as ITER. Experiments have been conducted using PISCES-B to simulate this effect and data have been analyzed by WBC Monte Carlo code [1] in collaboration with ANL.

In the PISCES experiments, a small piece of Mo is embedded as the marker "impurity" at the center of a graphite plate with a diamter of 5 cm. Experiments are currently conducted in two configurations: (1) normal incidence; and (2) non-normal incidence of the magnetic field on the graphite plate. Argon plasmas with a magnetic field of 500 Gauss, a plasma density of around 2×10^{12} cm^{-3} and an electron temperature of about 17 eV are used for these experiments. The ion bombarding flux is about 8×10^{17} $ions/cm^2/s$ and the ion bombarding energy is controlled in the range from -100 to -150 eV by applying a negative dc-bias on the graphite plate. Under these conditions, sputtered Mo is ionized with a mean free path of about 2 cm and the averaged gyro-radius of Mo^+ is about 9 cm. From these calculations, the probability of Mo ion redeposition is calculated to be about 15 % using the WBC code.

In the case of configuration (1) postbombardment surface analysis using EDX has indicated that, in general, the Mo concentration decreases exponentially from the center towards the edge of the graphite plate. At each radial position, however, the Mo concentration tends to saturate after a plasma fluence of about 1.4×10^{21} $ions/cm^2$. This indicates that although one expects a constant flow of Mo, an equilibrium composition may be established. The exponential radial profile is well predicted by the WBC code. Also, it is found that the observed concentration at equilibrium can numerically be estimated, assuming the formation of a carbon/molybdenum overlayer on the graphite plate. This is becuase such surface layers have been found to reduce sputtering of Mo significantly at elevated temperatures [2], which can then result in an "apparent" equilibrium composition.

[1] J.Brooks, Phys. Fluids. B 2(8) (1990)1858.
[2] K.Morita, Fusion Technol. 19(1991)2083.

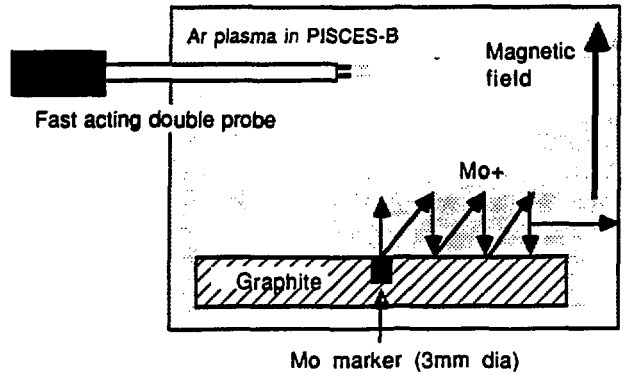

Figure 1 A schematic diagram of the experimental setup.

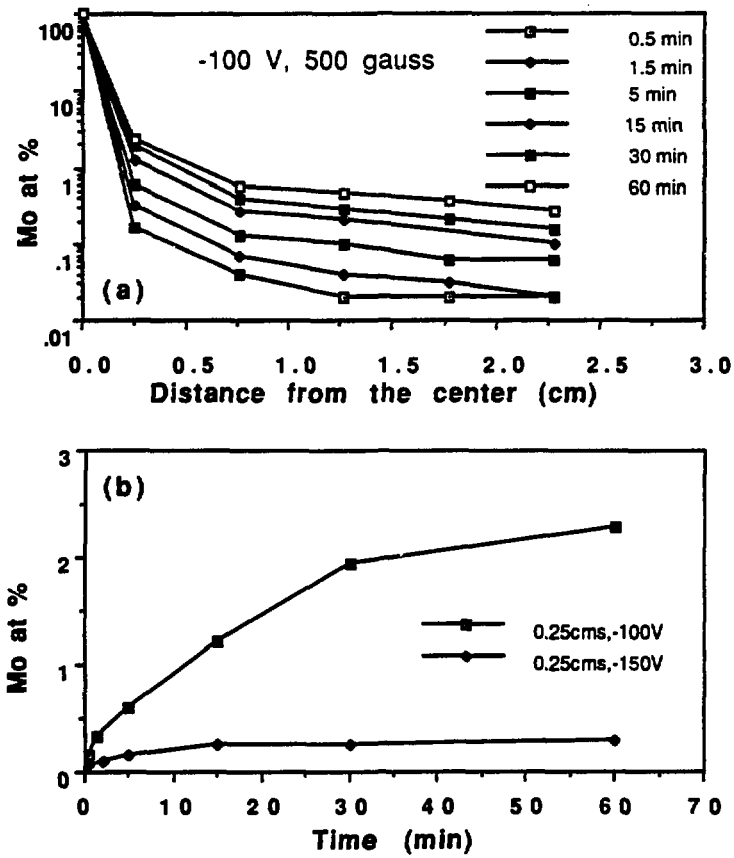

Figure 2 a) Mo radial conc. profile at 500G, -100V bias
b) Variation in Mo conc. with bomb. time.

4. PISCES Experiments

-Edge Plasma Physics-

Heat Flux Reduction and Impurity Screening in a Gas Target Divertor

(Simulation Experiments in PISCES-A)

Management of the divertor heat-load deposition is a critical issue for the design of next generation fusion devices such as ITER. The heat load to the outer divertor region is estimated to reach values of up to 50 MW/cm^2 in ITER during the technology phase. The severe erosion and impurity control problems at these power levels have stimulated research on alternative divertor concepts. The idea of the reentrant divertor is to redistribute the divertor heat flux over a large surface area by radiation and/or elastic and inelastic collisions with neutral particles. A wide range of experiments has been performed in PISCES-A to simulate a divertor plasma interacting with a neutral gas target and to evaluate the relevant atomic physics and plasma transport processes [1]. Recent experiments have focused on obtaining a high density hydrogen plasma with electron temperatures in excess of 15 eV, with the goal to produce ITER-relevant heat flux to the simulated divertor target.

The basic set-up of the gaseous divertor simulation experiment in PISCES is shown in Fig. 1. Downstream at a distance of about 1 m from the plasma source, the flowing plasma is accepted in a water-cooled circular neutralizer tube. The axial magnetic field can be varied from 0.4 - 1.7 kG. The simulated divertor target is located at the downstream side of the tube (z=0). The tube is made of anodized aluminum and is electrically floating. Neutral gas (H_2, D_2, He, Ar) can be fed from the end of the divertor tube. The neutral pressure in the plasma source can be kept well below 1 mtorr even at high secondary gas feed rates. An axially moveable Langmuir probe provides measurements of the electron temperature, plasma density and floating potential profiles along the length of the divertor tube. The chamber neutral pressure is measured with an ionization gauge, and the neutral pressure at two axial positions inside the tube (at distances z =1.5 cm and z = 41 cm from the divertor target) is recorded with ionization and baratron gauges. A CID camera as well as a 1.3 m Czerny Turner spectrometer with a photomultiplier tube is used to analyze plasma and neutral line radiation. A fast scanning, pneumatic Langmuir probe is used to obtain radial profiles of the plasma density and the space potential at select axial positions. A multitip radial probe is used to obtain the density and potential fluctuations $\tilde{N}$ and $\tilde{\phi}$ as a function of plasma radius. The radial particle flux driven by fluctuating electric fields is evaluated from the probe signals.

Previous experiments with hydrogen and argon gas targets have shown that a neutral density of 10^{14} -10^{15} cm^{-3} inside the plasma is necessary to access the "gas target" regime (where the electron temperature as well as the plasma density are decreasing

towards the target).[1] At the high densities expected in the ITER divertor region (n_e = 10^{14} - 10^{15} cm^{-3}) the neutral ionization mean free path is much smaller than the plasma diameter and the plasma is almost opaque to hydrogen neutrals (or injected impurity neutrals such as neon or argon). In turn, a fairly high gas pressure (p_n < 1 -10 torr) is required at the plasma periphery in order to maintain the required no inside the plasma column.

We have demonstrated access to the gas target regime for plasma densities as high as 5x 10^{13} cm^{-3} (kT_e < 15 eV). Improved differential pumping in the plasma source as well as a particular plasma start-up sequence are critical to achieve these parameters. Typical axial profiles of the electron temperature, the plasma density and the neutral pressure P_n in the "neutralizer" regime are presented in Fig. 2. The magnetic field is 1.7 kG. Here, the hydrogen neutral pressure reaches 0.18 torr close to the target at the end of the neutralizer tube. For reference, the neutral pressure measured with the plasma shut off, P_{n0}, is also shown. The pressure increase (a factor of 2.7) is due to plasma pumping effects. The maximum heat flux measured upstream close to the tube entrance exceeds 3 MW/m^2 (corresponding to one fifth of the ITER divertor heat flux during the physics phase). The electron temperature is observed to decay from kT_e=13 eV close to the tube entrance (z=90 cm, not shown) to kT_e =2 eV at the divertor target. This corresponds to a heat flux reduction of 94 %. The plasma density presently achieved is limited by tolerable the heat load to the (water-cooled) probe diagnostics. We expect to be able to operate close to n_e = 10^{14} cm^{-3} if fast injection probes are used.

Impurity injection experiments have been carried out to evaluate the potential of the gas target divertor for impurity screening. A trace amount of argon has been injected through the target plate. The argon neutral and ion density can then be estimated from spectroscopic line intensity measurements at different positions along the neutralizer tube. Figs. 3 and 4 show the normalized line intensities I/n_e of two argon lines (Ar II at 4805 A, and Ar I at 7504 A), measured at z = 42 cm, as a function of the averaged plasma density. The argon injection rate was kept constant. The local argon neutral and ion densities are approximately proportional to I/n_e, since the electron temperature at this location is fairly insensitive to the plasma conditions. A dramatic reduction of the impurity concentrations with increasing plasma density is observed, indicating effective impurity screening.

---

[1] L. Schmitz, et al., J.Nucl.Mater. 176&177 (1990) 522

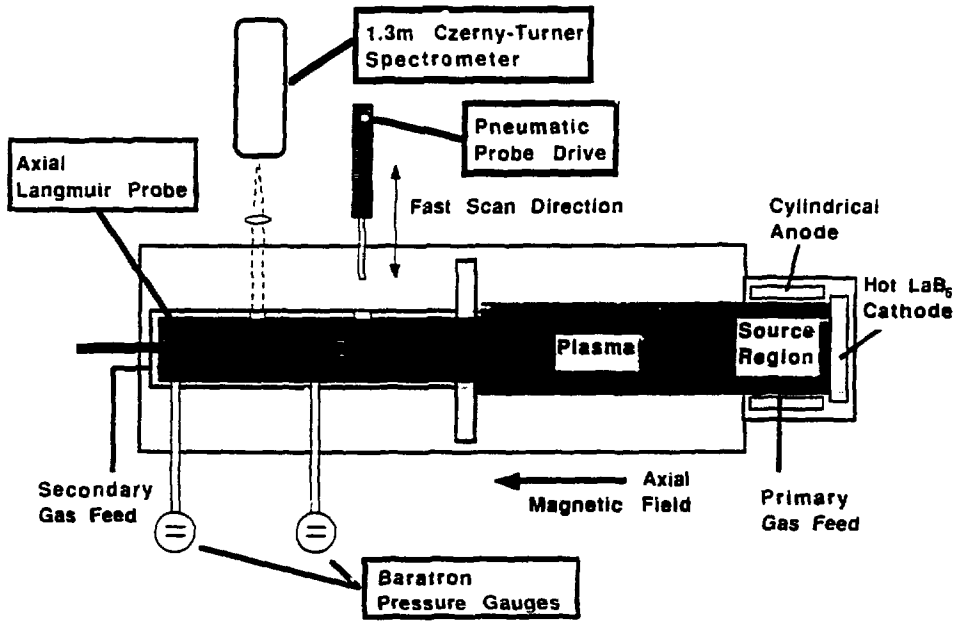

Fig. 1 Schematic of the experimental set-up for the gaseous divertor simulation in PISCES-A, showing the plasma source, the neutralizer tube and various diagnostics.

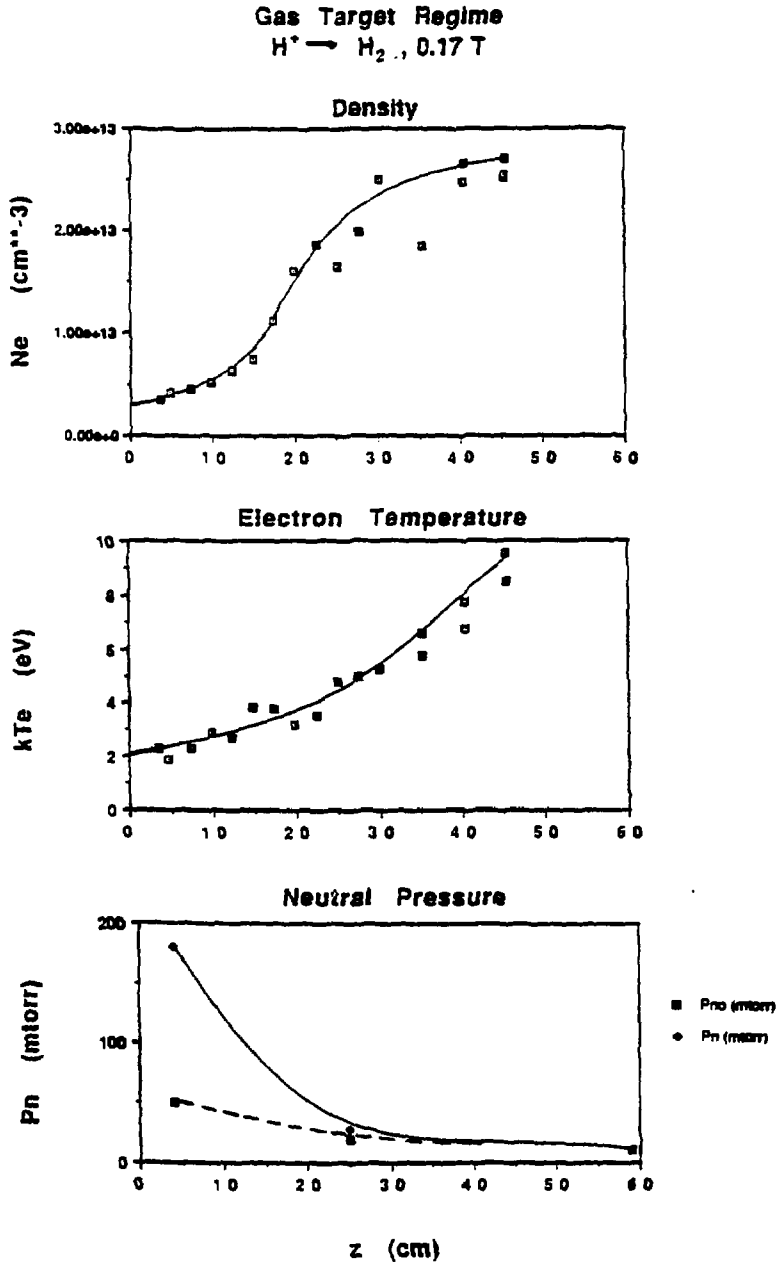

Fig. 2 Axial profiles of the plasma density, electron temperature, and neutral pressure in the in the gas target regime; a high density hydrogen plasma is injected from the right. The simulated divertor target is located at z=0; the neutralizer tube entrance is at z=90 cm (not shown).

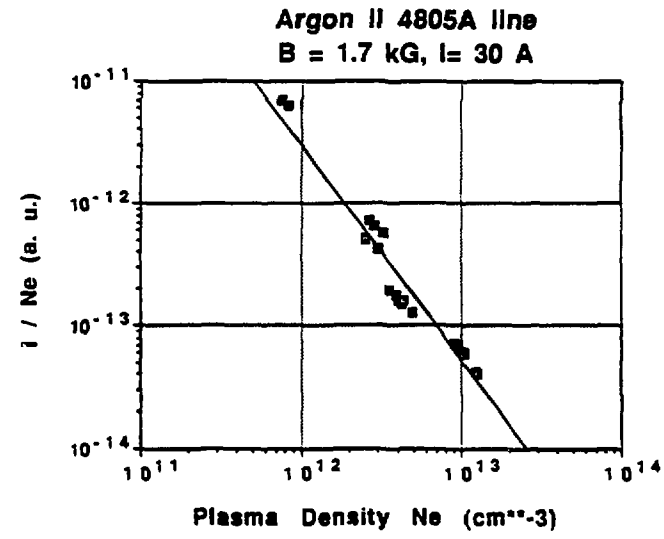

Fig. 3 Normalized line intensity I/n_e of the argon ion line at 4805 A (or relative argon ion density), measured at z = 42 cm, as a function of the averaged plasma density.

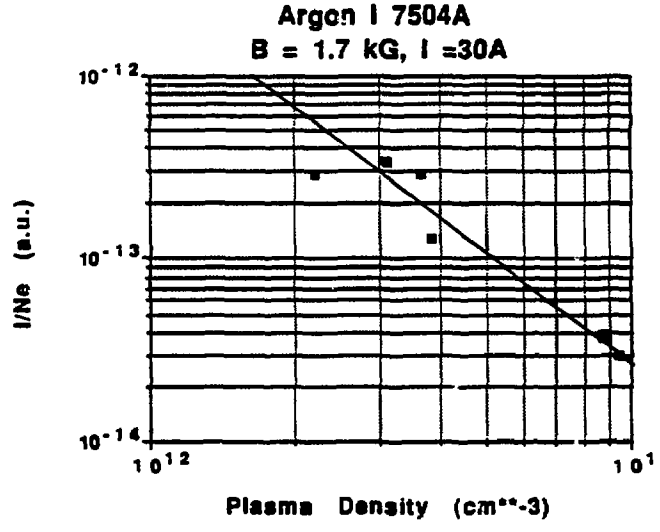

Fig. 4 Normalized line intensity I/n_e of the neutral argon line at 7504 A (or relative argon neutral density), measured at z = 42 cm, as a function of the averaged plasma density.

PISCES-CCT Edge Physics Collaboration

The PISCES-CCT edge physics collaboration has continued during 1991. In this work, tokamak edge plasma transport physics are being studied using an extensive poloidal probe array (P^2A) diagnostic that has been constructed and installed on the CCT tokamak (Fig. 1). The probe array can measure equilibrium plasma density, electron temperature and plasma potential as well as the edge plasma fluctuations. In this way, a comprehensive picture of edge plasma transport is being constructed.

A number of significant findings emerged from this work during 1991 and are listed below in an abbreviated form.

- Large-scale, large amplitude convective cells have been found inside the limiter radius, i.e. in the edge region of the plasma core. The maximum convective velocity is nearly one half of the local sound speed.

- A correlation between the large-scale convection pattern and the local turbulence levels and turbulent-driven particle transport is observed.

- An order-of-magnitude poloidal variation in the turbulent-driven particle transport exists. Nearly all of the transport occurs in the region characterized by magnetic field lines with 'bad-curvature'.

- Changes in the radial density decay length corresponding to variations in the cross-field particle fluxes are observed. Significant poloidal variations of plasma density and electron temperature are also found. Density and electron temperature vary by a factor of two at the last closed magnetic surface. These variations correspond to the poloidal distribution of radial particle transport.

Data illustrating the first point is shown in Fig. 2. Here, the P^2A diagnostic has been used to measure the two-dimensional plasma potential distribution $\phi_{pl}(r,\theta)$. Large amplitude ($\Delta\phi \sim k_B T_e/e$) time-stationary plasma potential maxima are localized radially to the region around limiter radius ($r/a=1$). These potential maxima have a significant ($\Delta r/a \sim .1$) radial width (here a is the plasma minor radius) and are elongated in the poloidal direction (poloidal mode number $m \sim 4$ - 5). These structures are stationary in the laboratory frame. Their structure may change with a change in plasma current, toroidal magnetic field, and/or edge safety factor q_a. The resulting electric field has both radial and poloidal components and hence will induce a particle drift of the edge plasma. Since the spatial scale of the potential distribution is much larger than the particle gyroradius, the potential contours then correspond to the ExB flow streamlines. The maximum flow speed is nearly half the local ion-acoustic speed.

These large scale convective patterns modulate the local microturbulence amplitude as well. The root-mean-square fluctuating poloidal electric field amplitude is shown in Fig. 3. The data indicate that the turbulent electric field fluctuations are largest at the interface between adjacent large-scale convective patterns. This suggests that the convective patterns are a driving source for the turbulent fluctuations. In this scenario, the large-scale convective patterns decay and generate small-scaled vortices which are damped as they propagate away from the excitation region. Additional analysis and measurements are needed to confirm this physical picture.

Large-scale convection is the dominant particle transport mechanism inside the limiter radius in CCT. At the limiter radius both turbulent particle transport and large scale convection are important transport processes. In the scrape-off layer, turbulent transport is the dominant particle transport mechanism. In CCT the total radial transport of particles varies significantly with poloidal position. Variations in the local density and electron temperature that correspond to the local radial transport rate are also observed.

These results indicate that flux-surface averaged pictures of transport present a limited view of tokamak transport. Additional measurements in CCT are needed to study the origin of the convective cells and to confirm the relationship between large scale convection and small scale plasma turbulence. Two-dimensional flow visualization techniques should be tried in CCT to make a direct observation of the convective patterns. A search for similar convective patterns in other tokamaks is also being planned and initial experiments will be performed on the TEXTOR tokamak during late 1991 and early 1992. If such patterns are found in TEXTOR, then large-scale convection may prove to be an important transport mechanism that exists in all tokamak devices.

Relevant publications
[1] G.R.Tynan, "Two-dimensional particle transport in the CCT tokamak edge plasma" UCLA-PPG-1369, June 1991.
[2] G.R.Tynan et al. "Steady-state convection and fluctuation-driven particle transport in the H-mode transition" to be published in Phys.Rev.Lett.
[3] G.R.Tynan et al. Bull. APS 36:9 2500(1991).
[4] G.R.Tynan et al. Proc. on 18th Euro. Conf. on Controlled Fusion and Plasma Physics, June 1991 Berlin, FGR, VIII, p 89.

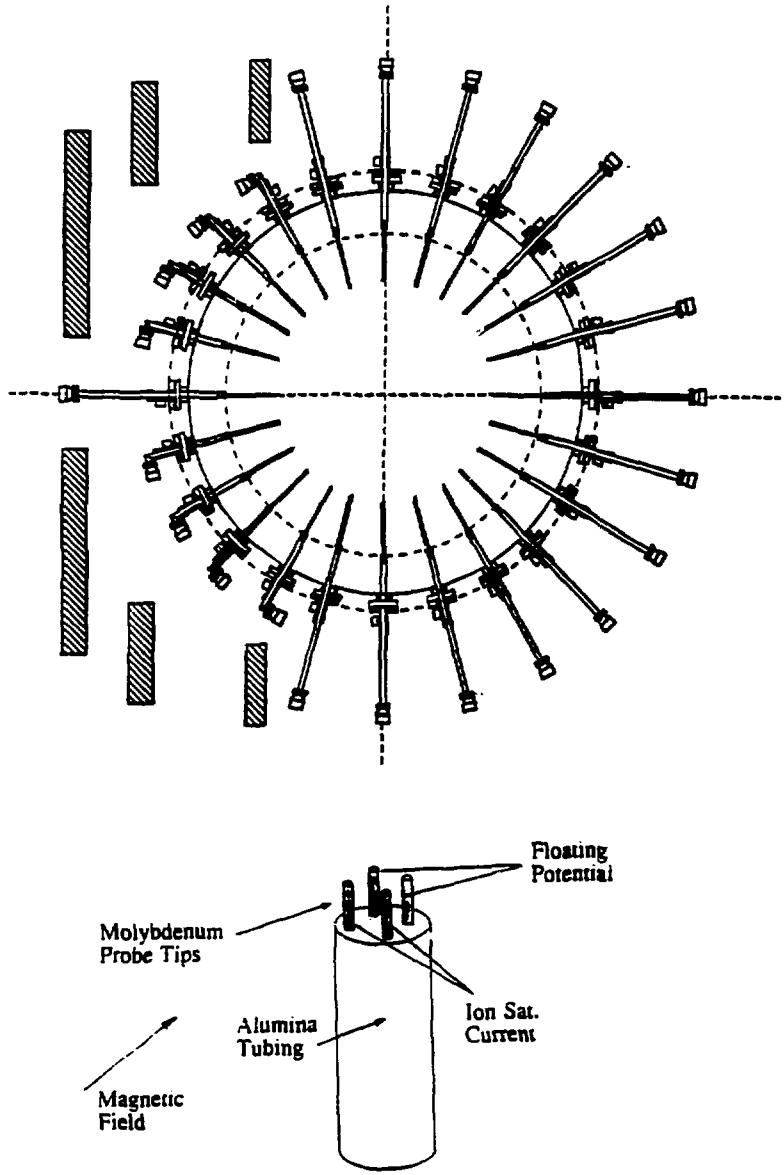

Figure 1: CCT Poloidal Probe Array and Probe Tip Details

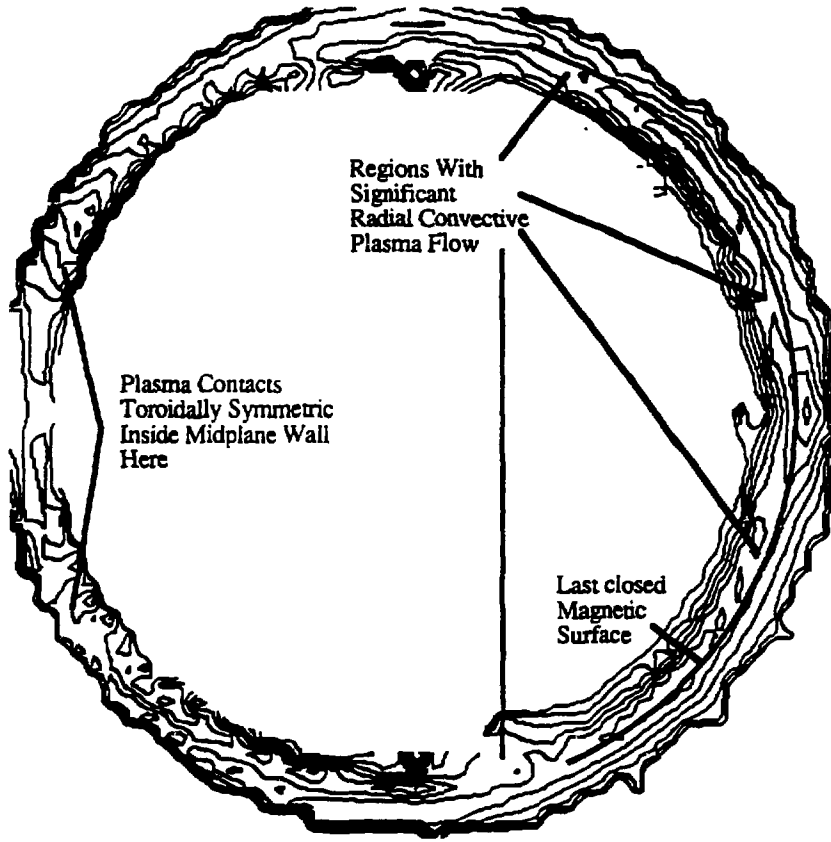

Figure 2: Time-averaged plasma potential radial and poloidal distribution in the edge plasma region of the CCT tokamak (15V contours shown). Outside midplane is to the right in the figure. Data from measured floating potential and electron temperature distribution. The results indicate the presence of large-scale stationary electric fields in the edge plasma region. These electric fields induce ExB plasma drifts in the radial and poloidal directions.

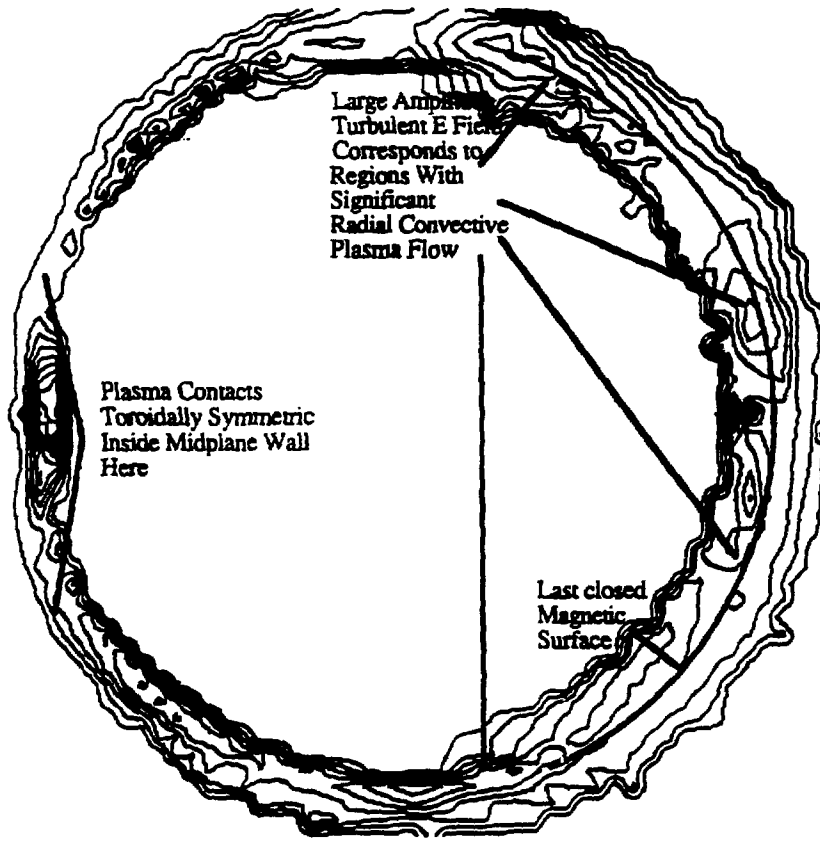

Figure 3: Radial and poloidal distribution of the root-mean-squared fluctuation poloidal electric field (4 V/cm contours shown). Outside midplane is to the right in the figure. The $\tilde{E}_\theta$ amplitude is largest at the periphery of the convective patterns and at the interface between adjacent convective patterns. This suggests that the plasma turbulence is driven, at 21least in part, by the large-scale plasma flow.

Ongoing research on the L to H mode transition in tokamaks has centered on the radial electric field as being the controlling factor in the transition. The magnitude of the electric field, or the strength of the shear in the field, can dramatically influence the nature of the electrostatic turbulence in the edge plasma. Furthermore, it has been suggested that the turbulent nature of the plasma controls the cross field heat and particle transport. Thus, the radial electric field can have a significant bearing on the rate of anomalous cross field diffusion.

PISCES provides an unique environment for studying the effects of radial electric fields on plasmas with conditions similar to tokamak edge plasmas. Steady state discharges are studied with probe arrays, either mounted on pneumatic carriages or fixed in the plasma dump. Spectroscopic means for monitoring the turbulence are also available. Because of the strong negative potential applied to the cathode in a reflex arc discharge, an inwardly pointing radial electric field is present even without an applying a bias to the plasma periphery. Using an annular electrode mounted on a limiting aperture plate (Figure 1), the existing electric field can be modified and the peak electric field strength has been observed in excess of 100V/cm. The radial electric field is increased when a large electron current is drawn to the annular electrode. When this strong electron current is drawn, the radial electric field is peaked near the aperture radius (Figure 2a) and the central plasma density increases (Figure 2b). In addition, the density scrape-off length decreases significantly when the bias is applied. From the measured potential profiles, a poloidal flow profile can be inferred, and when the bias is not applied, a natural single shear layer exists just inside of the aperture radius. When the electron current is drawn, this layer is modified to a double shear layer, with a strong jet of plasma rotating poloidally just inside the aperture radius.

The nature of the turbulence and the turbulent driven particle flux also change dramatically between the single and double shear layer cases. In the double shear layer case, both the density and potential fluctuation levels decrease in the scrape-off layer (Figures 2c-d), while the density fluctuation levels are not modified significantly in the central plasma column. The turbulent driven particle flux is inferred from the strength of and phase between the fluctuating poloidal electric field and density. Temperature fluctuations are not taken into account and are considered negligible. The turbulent driven particle flux is decreased by 30 to 90% when the double shear layer is formed (Figure 2e), due mostly to a suppression of the turbulence rather than a change in the phase between the density and electric field fluctuations. From a spectral analysis of the potential fluctuations

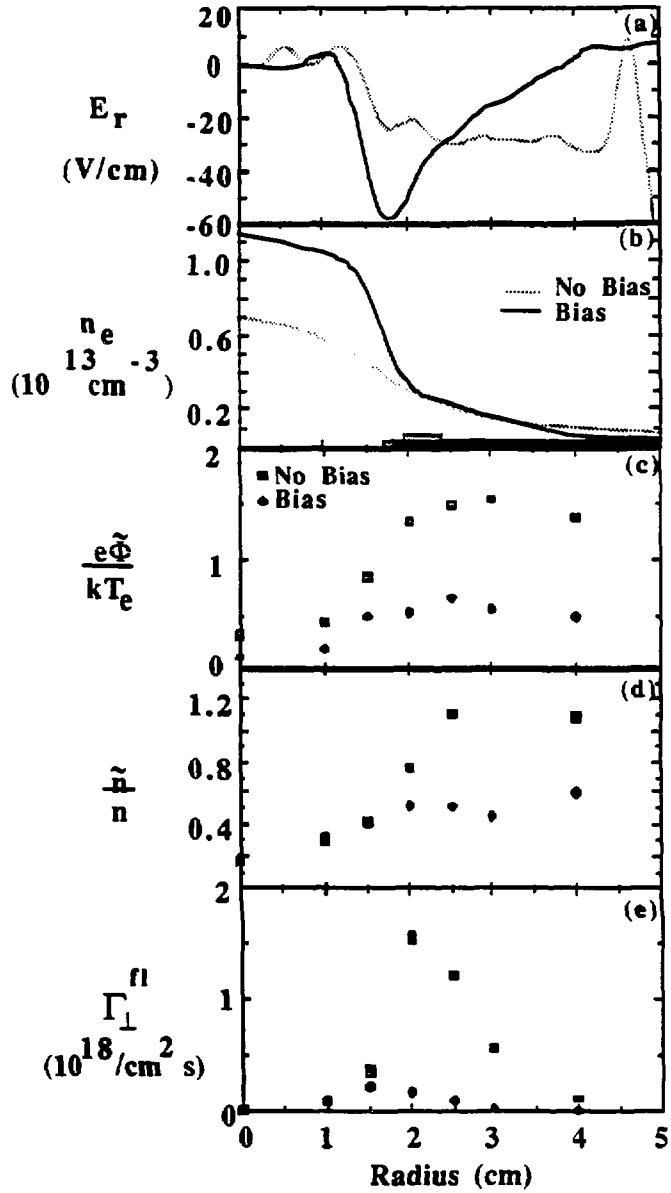

Figure 2: Radial profiles comparing unbiased and strongly biased conditions: (a) radial electric field, (b) plasma density, (c) potential fluctuations, (d) density fluctuations, and (e) turbulent-driven particle flux.

from the poloidally separated probes, as well as a radially staggered probe, both the poloidal and radial correlation lengths at the aperture radius are seen to decrease when a double shear layer exists. This suggests that small turbulent eddies are being stretched and torn in the strong poloidal jet that forms when the bias is applied.

Future work will include a search for coherent fluctuations using conditional sampling techniques. Scalings of the turbulent properties with neutral pressure, magnetic field, and electric field strength and shear are continuing. The ongoing edge plasma modelling effort at UCLA continues to use data provided by PISCES.

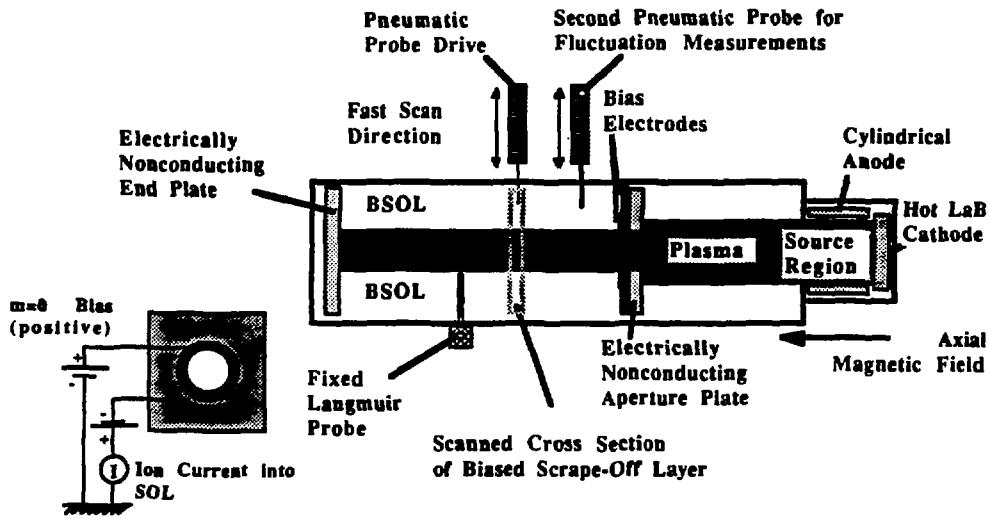

Figure 1: Schematic diagram of the experimental setup for the bias experiments in PISCES-A.

H-Mode Transition Physics-II: Observation of Steady State Convection

Turbulent fluctuations are not the only mechanism that has been proposed to control the cross field heat and particle transport in tokamak edge plasmas. It has been conjectured that steady state or long lived coherent structures may be responsible for some of the poloidal asymmetries observed in tokamaks. These coherent structures can also contribute to the particle and heat transport through non-diffusive transport processes such as convection. In addition, the convective patterns can also stimulate electrostatic turbulence, which in turn produces turbulent driven transport. Since convective patterns are difficult to map out, studying them under controlled conditions may shed some light on their contribution to heat and particle transport, as well as the L to H mode transition.

Convective patterns can be studied under the same conditions as the turbulence experiments described previously. Steady state discharges in PISCES are scanned with a pneumatic fast scanning probe mounted on a sliding O-ring seal. Two dimensional profiles of the plasma potential and density are created by accumulating successive shots while moving the probe carriage perpendicularly to the axis of the plasma column. The strength of the radial electric field can be modified by applying a bias to an annular ring electrode just outside of the aperture radius. Figure 1 shows the two dimensional plasma potential and density profiles when no bias is applied to the annular electrode. Because of the strong negative potential applied to the cathode in a reflex arc discharge, the potential in the central region of the discharge is depressed. Since the equipotential and equi-density contours are not cylindrically symmetric outside of the central plasma column, large scale, steady state convective cells are seen to be present. Figure 2 shows the same two dimensional profiles when a strong electron current is drawn to the annular electrode and a stronger radial electric field is produced. The contour plots show that the poloidal asymmetries in the potential and density are minimized when the stronger radial electric field is applied. The reduction of poloidal asymmetries coincides with a decrease in turbulence levels and reduction in the total radial particle transport.

Future work will concentrate on visualizing convective patterns with both a grid of Langmuir probes and conditional sampling techniques. Improvements in the control and stability of the discharge will be made to minimize shot to shot variations that limit the resolution of the existing experimental technique. Changes in convective cell structure due to changes in edge density gradients and the shear in the radial electric field will be studied to better understand the impact on transport barrier formation during tokamak H-modes.

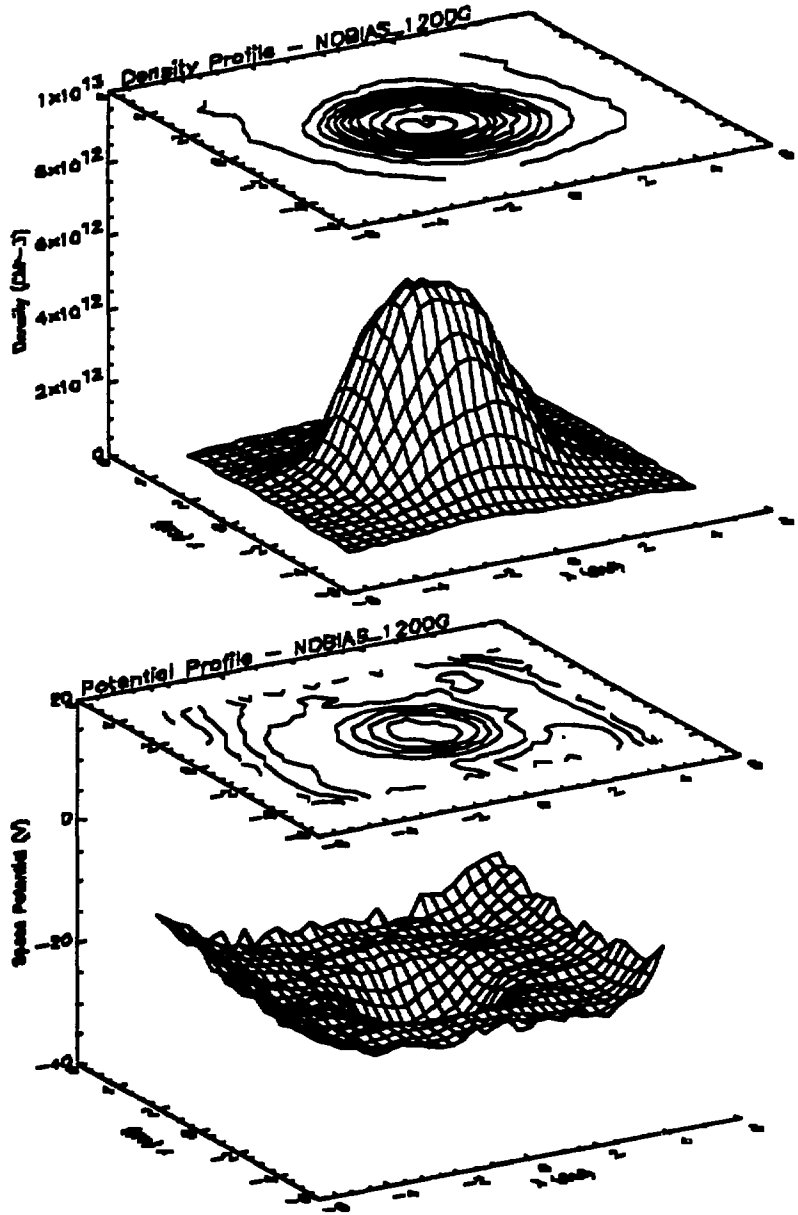

Figure 1: Density and potential profiles without biasing. Poloidal asymmetries are observed in both the density and potential profiles.

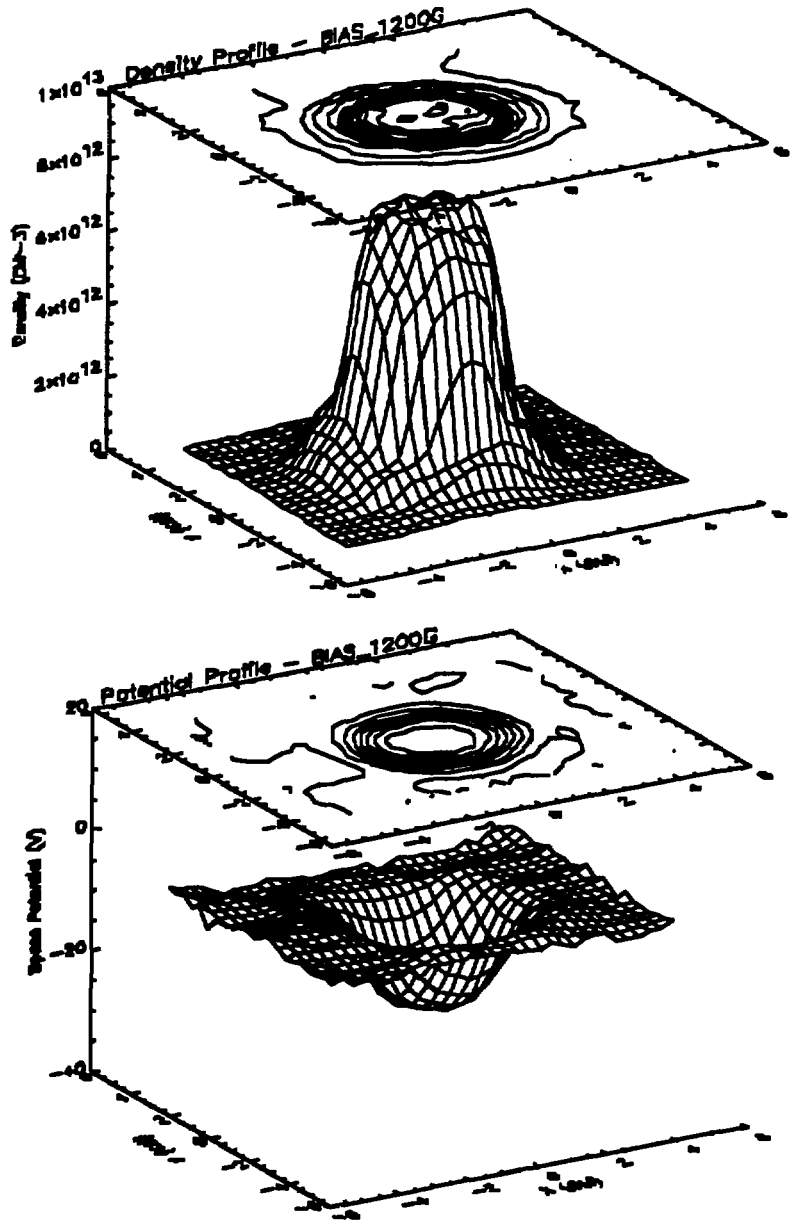

Figure 2: Density and potential profiles during strong biasing. Density and electric field profile in scrape-off layer steepen and poloidal asymmetries are minimized.

5. Theoretical Analysis

-Edge Plasma Behavior-

H-mode Physics-III: Plasma Behavior in a Sheared Electric Field

Recent tokamak H-mode experiments indicate that a strong radial electric field is formed at the plasma edge during the transition between L-mode and H-mode confinement. This radial electric field is radially localized in a narrow region and leads to a highly sheared ExB plasma flow. Simulation experiments currently being performed in the PISCES-A linear device, indicate that the fluctuation level and fluctuation induced particle transport are reduced when a strong, double shear layer (DS) is produced by biasing the plasma boundary layer, whereas the turbulence level and transport is rather high in the case of a weak single shear layer (SS) (observed when no bias is applied).

The source of the turbulence in SS cases is thought to be the Kelvin-Helmholtz instability (K-H), since the results of the experiments have shown some characteristic properties of this instability. Considering that larger shear and two shear layers are the major differences between the DS and SS cases, the following analytical and numerical simulation work is being performed to understand the dominant physics involved in these experiments.

(1) The kinetic equilibrium of plasma in a strongly sheared electric field

Since the driving source for the K-H is the sheared flow of plasma rather than the sheared electric field, correct information about the plasma response to a sheared electric field is needed. Usually, a plasma (in a uniform magnetic field B_z) is thought to respond with a steady state ExB drift to an electric field. This is true for the case where the electric field is uniform and weak, and the time scale of interest is much larger than the ion gyro-period. However, the plasma responds in a different way if the electric field has a large spatial gradient or the time scale of interest is shorter than the ion gyro-period.

A set of implicit expressions is derived for the motion of a single ion in an arbitrarily sheared electric field (the field and its gradient in x-direction are prescribed) . The motion of an ion in a highly sheared electric field is evaluated numerically. When a linear spatial variation of an electric field is considered, the plasma has the following response. (a) if the gradient of the electric field is in the +x direction, the motion of an ion is always periodic but with a larger frequency (called 'shear gyro-freqency' in this report), which is the sum of the gyro-frequency and the 'shear frequency' (defined as the gradient of the ExB drift velocity). The concept of periodic motion around a drifting guiding center still applies, but the drift speed is different from normal the ExB drift speed (very different if the shear frequency is comparable to the gyro-frequency). For the purpose of investigating the K-H instability, approximation of a steady drifting plasma equilibrium with the new drift velocity is roughly valid. (b) If the gradient of the E-field is in the -x

direction, the motion of an ion is very different from the ExB drift motion. The ion may experience no drift, or drift in a direction opposite to the normal ExB drift. In our DS experiments, one of the two shear layers exhibits this behavior.

(2) Interaction between two K-H unstable regions

If a steady ExB drift is assumed to be the response of plasma to an electric field, a double shear layer implies two sheared plasma layers with sheared flow and each layer will drive a K-H type instability . Thus two K-H instabilities will be driven initially in DS cases, while only one will exist in the SS case. To understand the effect of the interaction between the two regions, a linear analysis has been done using a fluid model. The results show that for nonsymmetric double shear layers, this effect reduces the growth rate of the K-H instability driven in the layer with the larger shear frequency while increasing the growth rate of the other K-H mode. For symmetric double shear drift layers, the growth rates of both K-H modes are reduced , and the effect is more significant. More detailed analysis of such interaction is under way by means of a particle simulation.

(3) Particle simulation

Since we are dealing with a nonuniform, bounded plasma, and have to take into account significant effects from the finite shear frequency and finite Larmor radius effects, an analytical approach is insufficient. And since we wish to understand the nonlinear behavior of the plasma for comparison with experimental results, a fluid model clearly is not sufficient. Therefore we analyze the problem by means of a particle simulation , which preserves kinetic effects. The BEPS-2D code , written by Dr. Decyk of the UCLA Physics Department, has been modified to simulate these physical processes. The code is capable of analyzing electrostatic plasma behavior in two dimensions. Modifications include (a) the initial density can be nonuniform; (b) an SS or DS electric field can initially be entered and the electron density profile will automatically be adjusted to satisfy Poisson's equation; (c) plasma can be nonneutral; (d) the equilibrium electric field can be maintained during the entire simulation; (e) the initial velocity distribution function is Maxwellian with a superimposed local drift speed. Convective cells driven by m=2 and m=3 K-H modes have been observed during test runs of this code for weak double shear layer cases. The results will be compared with the PISCES-A experimental results and should provide additional insight into the physics of cross-field plasma transport in highly sheared plasma flow layers.

Edge Plasma Control By RF Ponderomotive Forces and Electrostatic Bias

The peak power load and erosion of a divertor plate is governed by the area on the divertor plate over which power is deposited. That area is in turn governed by the scrape-off layer length which expresses the balance between cross-field transport (leakage out of the magnetic bottle) and flow of plasma parallel to magnetic field lines to the divertor or limiter. To reduce the peak power load and erosion, it is beneficial to alter this transport balance. Experiments in PISCES have shown that the particle transport in a tokamak can be significantly altered by externally imposing an electrical potential to limiter and/or wall surfaces, or by imposing a ponderomotive potential within the plasma from an RF source. In this research, we have developed for the first time an analytic and numeric transport model which includes both ponderomotive[1] and electrostatic potentials[2]. This model helps us understand mechanisms responsible for the transport physics properties of the plasma in an ordinary scrape-off layer, as well as a scrape-off layer having ponderomotive potentials and biased surfaces. Moreover, in most of the experiments, the confinement properties of the core plasma also change, leading to the conclusion that not only does the potential influence transport in the SOL, but also on the closed magnetic flux surfaces near the plasma velocity. To understand this effect, a fully ionized transport model, appropriate for the core has been developed in parallel with the SOL model, we anticpate combining the two models in the near future. A separate, but related issue is the degree to which non-ambipolar transport can be supported by the the SOL plasma. Unlike the core, cross-field electron and ion fluxes are not constrained to be ambipolar within the SOL. Currents may flow along field lines through the limiter, an effect which is enhanced by limiter biasing. Even in the absence of an externally applied bias, currents can arise in the SOL from such diverse mechanisms as differences in electron temperature, differences in potential due to drift effects and magnetically induced electric fields. In turbulence-free plasmas, these non-ambipolar boundary conditions can modify the density profiles that would ordinarily occur in an ambipolar plasma. In the presence of turbulence, this effect is not so clear, and to investigate it further, we have included such nonambipolar effects within the framework of a phenomenlogical model of edge density and potential fluctuation effects. Since neutral-plasma interaction can play an important role, particularly in cases where the local ionization is important, such as high recycling or gas divertor plasmas, we have included within the model particle sources, including atomic and ionization cross-section calculations. We sought a model which would apply equally well to tokamak geometry as well as simple cylindrical geometry, such as encountered in the PISCES linear edge simulator, so while a basic cylindrical coordinate system is utilized, we retain terms which arise from taking the gradient of the magnetic field, including curvature and radial inhomgeneity. The model is sufficiently general, that any

[1] T. Shoji, A.A. Grossman, R.W. Conn, et al., J. Nucl. Mater. **176-177** (1991) 830.
[2] B. LaBombard, A.A. Grossman, R.W. Conn, J. Nucl. Mater. **176-177** (1991) 548.

of these mechanisms can be "turned off" and used to understand transport due to the remaining mechanisms. Thus the calculation can be used to design an "RF ponderomotive divertor", a "biased divertor/limiter" or an ordinary scrape-off layer plasma without any biasing or ponderomotive potentials. The analytic model is 1-D, allows for biasing and ponderomotive potentials, uniform neutral sources, and provides a simple ordinary differential equation for the transverse density and electric potential profile in the plasma. These ODE's are solved for the density and potential profile and the conditions under which the density profile is a simple exponential described by a characteristic scrape-off layer length are found. The model clearly demonstrates how either an electrostatic bias or a ponderomotive potential can be used to change this scrape-off layer length. To treat the more general 2-dimensional geometry, including toroidal effects and drifts, a set of coupled partial differential equations are derived which describe density and electrostatic potential. Fluctuation driven transport is included by assuming the density and potentials have an average and a fluctuating term and resulting equations are averaged so that only correlations produce transport which are folded into a phenomenlogical anomalous diffusion coefficient. Terms coming from taking the gradient of the magnetic field are retained, so that the model can be used to describe tokamak transport. These magnetic field terms arise from the E X B, diamagnetic, and ponderomotive force X B drifts, and are fully retained in the model. The equations are finite differenced on a two dimensional grid and solved numerically for the density and potential distributions everywhere in the plasma, using standard matrix LU decomposition techniques. Boundary conditions include either the specification of density and potential (Dirichlet) or their derivatives (Neumann) or any combination at the boundary. Nonlinearities in the potential calculation are treated by standard Newtonian iteration techniques. At every iteration, a plasma potential is calculated, from which is obtained a floating potential at each node. Depending on the value of this floating potential relative to the biased surface, there will be a current flowing between plasma and the wall. With an additional iteration loop, we impose the condition of global ambipolarity which requires that overall this current be zero, so that even thought locally there may be currents floating, overall the net current is zero. This model is designed to allow detailed comparison with experiments that have been performed on the PISCES linear edge simulator, as well as experiments underway or planned in tokamaks, which include both biasing and RF ponderomotive divertor. An example of the output from this code for the PISCES experiment is given in Fig. (1a,b) which gives contours of constant flux to the plate (a) without an applied RF (peak flux $6 \times 10^{18} cm^{-2} sec^{-1}$, and (b) with an applied RF field with ponderomotive potential of some 20eV, and a peak flux of $2 \times 10^{18} cm^{-2} sec^{-1}$. These and other calculations clearly indicate that the presence of a ponderomotive potential can have a considerable influence on the plasma density, potentials, and plasma flux to a surface.

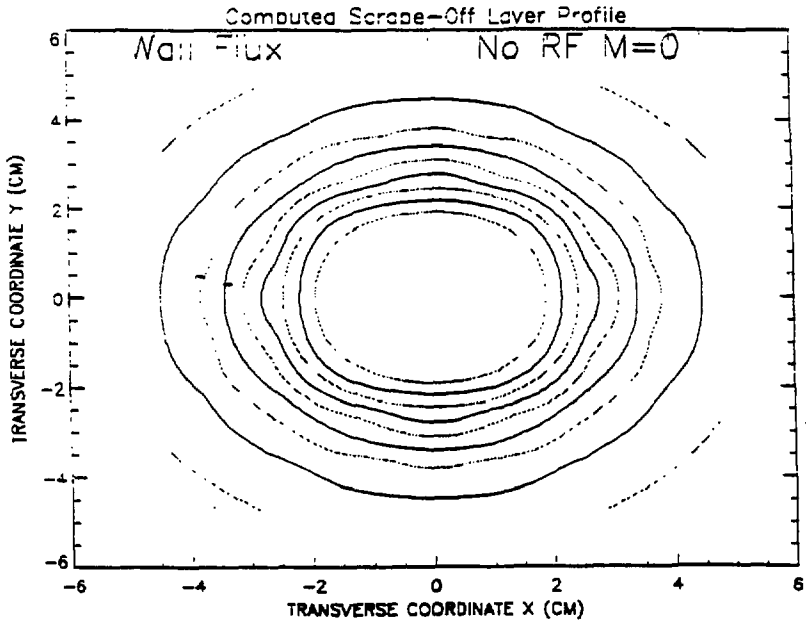

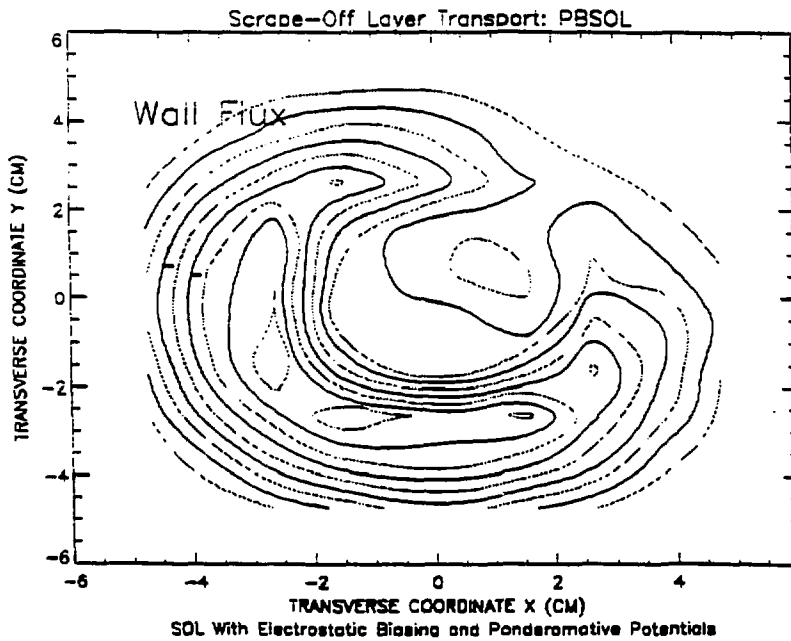

SOL With Electrostatic Biasing and Ponderomotive Potentials

Anormalous Boundary Plasma Transport by Subharmonic Electric Fields

In the gaseous diverter experiment in PISCES-A, it has been observed that the effective radial diffusion coefficient increases with increasing neutral gas density but is independent of the magnetic field in the range explored so far (< 0.2 T). The effective radial diffusion coefficient is larger than the Bohm coefficient and the classical ambipolar diffusion coefficient. It is postulated that the turbulent electrostatic fluctuations observed during the experiments may be responsible for this enhanced anomalous transport phenomenon. This theoretical analysis is intended to investigate the motion of a charged particle in a uniform magnetic field perturbed by an electrostatic field.

Depending on the magnitude of the perturbation, the particle motion can range from a small deviation from simple cyclotron motion to stochastic motion over the whole phase space. The latter case corresponds to anomalous transport. Thus, by studying the interaction between the particle motion and the perturbative electric field we may gain deeper insight into the particle transport mechanism.

The classical equation of motion for a single particle gyrating around a magnetic field line has periodic analytical solutions. If the particle motion is perturbed by an electric field, then the particle motion may no longer be described by a closed analytical expression. Instead, depending on the strength of the perturbation, the particle may exhibit stochastic motion in phase space (x-v space). An example is the so-called ``kicked oscillator'' with Hamiltonian [1]

$$H=\frac{\dot{x}^2}{2}+\frac{\omega_0^2 x^2}{2}-\varepsilon\frac{\omega_0^2}{k}\cos kx\sum_{n=-\infty}^{\infty}\delta(t-nT_0) \qquad (1)$$

(where the mass is set to unity, ε is a dimensionless perturbation parameter, $T_0=2\pi/\Omega$ is the fundamental perturbation period and Ω is the fundamental perturbation frequency). Equation 1 corresponds to the motion of a charged particle in a uniform magnetic field in the z-direction with cyclotron frequency ω_0, and under the influence of the wave packet field traveling along the x-axis.

The evolution of Eq. (1) in phase space can display many interesting phenomena. For example, if the resonance condition is satisfied (Ω/ω_0 = integer), i.e., in the harmonic case, a stochastic web structure with an exponentially thin width for small values of perturbation strength appears [1], and this web structure extends throughout the whole phase space. A particle originally located within the stochastic web will diffuse along the stochastic web and may reach distant parts of the phase space [3]. This phenomenon, the so-called Arnold diffusion [2], is the most unexpected discovery in the theory of non-integrable Hamiltonian systems. Particles starting from low energy can be accelerated to

very high energy through interaction with a wave packet of limited energy. The subharmonic case (ω_0/Ω= integer), however, has not yet been investigated in detail.

The goal of the present work is to investigate the particle motion under the influence of a subharmonic field, i.e., the particle motion perturbed by a wave field with a frequency that is some fractional part of the ion cyclotron frequency. This case is frequently encountered in the tokamak boundary plasma. We consider the one-dimensional motion of a particle described by the equation

$$\ddot{x} + \omega_0^2 x = \frac{E_0}{m} \sin(kx - \Omega t) \qquad (2)$$

which describes particle motion under the influence of a perturbation field with frequencyΩ, perpendicular to a uniform magnetic field. By making an independent variable transformation $\tau = \omega_0 t$, we can normalize the time to the cyclotron period. The equation of motion then becomes

$$\ddot{x} + x = \varepsilon \sin(kx - n\tau) \qquad (3),$$

where $\varepsilon = e E_0/m\omega_0^2$ is the perturbation strength of the electrostatic field and $n = \Omega/\omega_0$ is the ratio of the perturbation frequency to the cyclotron frequency.

Figs. 1-3(a) show the trajectories of a particle in phase space as a function of time (x, v vs. t (= 0 to 48 π) plot). In Fig. 1-3(b), we show the phase trajectories in each cyclotron period superimposed in one cell for twenty-four consecutive periods (x, v vs.\ t (= 0 - 2 π)). Fig. 1 is the phase plot of the unperturbed case, that is, $\varepsilon = 0$, and as we expect, the particle just exhibits simple harmonic motion. Fig. 2-3 show the numerical solutions of Eq. (4) with $\varepsilon = 0.1$ and $k = 1$ Fig. 2(a) shows that the harmonic electric field only slightly perturbs the cyclotron orbit, while in Fig. 3(a) the subharmonic electric field strongly pushes the trajectory away from the circular motion. This point is illustrated more clearly in Figs.2-3(b). In Fig. 2(b), the particle motion traces out almost the same trajectory every 2π, while in Fig. 3(b) the trajectory breaks into four bands with finite widths. Due to this finite band width, the particle motion becomes stochastic. The position of the particle after a finite number of cyclotron periods can no longer be predicted accurately.

These results suggest that for the same parameters and perturbation strength, the subharmonic field can perturb the phase trajectory more effectively than the harmonic field. Therefore, the observed subharmonic electric fluctuations may greatly contribute to the anomalous particle transport in our experiments.

[1] V.V.Afanas'ev et.al. Phys.Lett.A151(1990)276.
[2] V.I.Arnold,"Mathematical Mothods of Classical Mechanics",Springer-Verlag, NY,1989.
[3] G.M.Zaskavsky et.al. "Weak Chaos and Quasi-Regular Patterns", Cambridge Press, 1991.

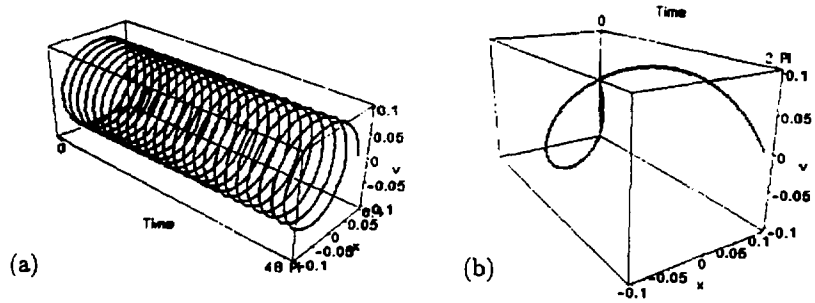

Figure 1: The cyclotron motion of a charged particle gyrating around a magnetic field line. with $\omega = 1$. $\Omega = 4$, $\varepsilon = 0$, and $k = 1$. The initial conditions are $(x_0, v_0) = (0.1, 0)$. Starting from $t = 0$ to 48π.

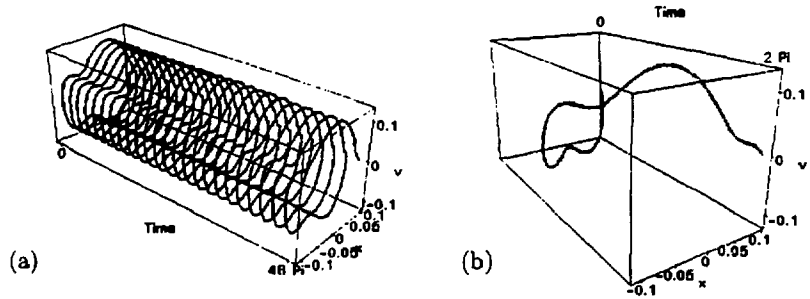

Figure 2: The particle motion under the influence of perturbative harmonic electric field with $\Omega = 4$ and $\varepsilon = 0.1$.

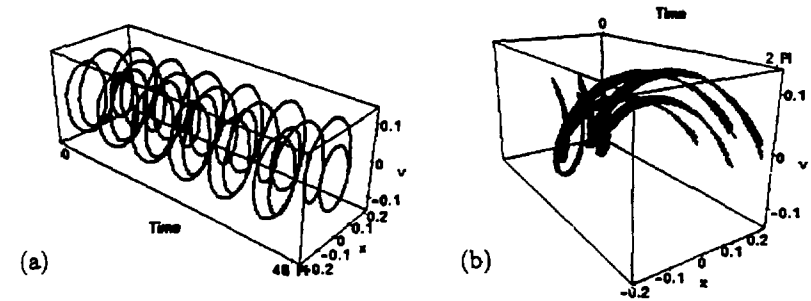

Figure 3: The particle motion under the influence of perturbative subharmonic electric field with $\Omega = 1/4$ and $\varepsilon = 0.1$.

Modeling and Optimization of Novel Edge Profile Modification Techniques

The PMI program at UCLA is directed towards understanding and modeling edge plasma phenomena and towards innovative solutions to design and operation of impurity control, particle exhaust, and plasma-facing components. We strive to produce a reliable and quantitative understanding of all the physical processes occurring in the edge plasma that are responsible for the experimental observations. Computational models developed for this purpose provide insight into the key issues of impurity and particle control, and therefore point towards areas where innovative solutions are needed. The codes additionally provide a mechanism by which to test and optimize these solutions under conditions expected in their application.

The first generation of two-dimensional edge-plasma simulations, such as the B2 and EPIC codes, demonstrated the value of fluid modeling of the SOL and they are currently used extensively for simulation of the divertor tokamaks. It should be mentioned that EPIC, the most complete model to date is the first U.S. two dimensional edge code and was developed at UCLA under our PMI grant. Even though the existing edge-plasma codes clearly established the need for this class of simulations, our experiences have also exposed many shortcomings of both the algorithms and user interfaces, and ultimately, the need for a second-generation simulation code. We have started work with advanced features toward this end. The aim is to develop a code which is easy to use, more accurate and includes improved physics models; but is also flexible enough such that it can be used for a range of machines from small laboratory experiments to full-scale fusion devices. Our technique represents a significant and necessary improvement over those employed in the available models, particularly in that computational grids are not forced to follow the poloidal magnetic flux surfaces, poloidal geometry is arbitrary, circulating flow is easily accommodated, and neutral physics at the vessel boundary are appropriately discretized. Finally, computational performance and user interfaces are drastically improved through state-of-the-art solution techniques and extensive menu--driven windowing software, respectively.

The work was centered first around the development an efficient solver for a generalized non-linear convection/diffusion equation with source terms. This is the mathematical form of all the fluid conservation laws for particle, momentum and energy transport, and its solution is the fundamental building block of any fluid edge plasma computation. The solver operates on arbitrarily shaped toroidally symmetric domains, essentially removing, for the first time, the dependence of calculated solution profiles on grid orientation and orthogonality. This has been accomplished by increasing the

information available to the solver about the local profiles, i.e. increasing the discretization stencil size to include more neighboring points. Next, a highly efficient algorithm is employed that can simultaneously solve a number of such equations, consistently capturing any coupling between the unknowns. The technique is based on well-behaved Newton-type iterations, optimally preconditioned for the special behavior of plasma flow, and is at least an order magnitude faster than previous methods. Using modern iterative linear matrix solving techniques in each Newton iterate, the entire code runs compactly and efficiently and does not require supercomputer resources. Finally, a user interface will be developed shortly that is built upon windowing software that operates transparently over most any desktop workstation or supercomputer available. The code that we produce will be fully portable to any system running standard FORTRAN 77, and made available for use and modification to the entire edge modeling community.

We have completed the development and testing of the generalized non-linear convection/diffusion equation solver. Results show that we have indeed met our goal to essentially eliminate grid orientation dependence of the solution. The strong anisotropic diffusion that is unique to magnetized plasma systems presents no particular difficulty for the scheme, and is in fact simulated quite nicely. Optimization of the preconditioned Newton algorithm has proceeded in parallel, and has enjoyed equal success. In a simplified three-equation set we have demonstrated a 15:1 reduction in the number of iterations required to reach a converged solution, without unduly stressing the memory or CPU requirements of our desktop machines.

The next step is to combine the two efforts, and finally to scale the generalized terms in each equation to represent processes extant in the physical system. Successful results from modeling the edge physics with the first-generation codes give us confidence that we indeed will capture the essential dynamics. But the present work allows far greater flexibility in the application of this work to engineering design and analysis of the available experimental data. Upon successful matching of plasma profiles measured in laboratory experiments such as PISCES, the identical code will be used, for example, to determine the effects of rather extreme geometry and state modifications; and ultimately for the recommendation of the most promising of full--scale reactor configurations.